Table IV. CA repeat polymorphism and lung cancer risk with adenocarcinoma histology among radiation dose-stratified populations

Genotype	*N.* cases/sub-cohort	RR1[a]	95% CI[b]	RR2[c]	95% CI[b]
Non-exposed					
Long	6/488	1.0[d]		1.0[d]	
Short	13/389	3.33	1.23–9.02	2.93	1.11–7.73
5–712 mGy[e]					
Long	9/343	1.0[d]		2.18	0.77–6.17
Short	6/256	0.94	0.34–2.66	2.02	0.65–6.31
≥712 mGy[e]					
Long	17/345	1.0[d]		4.37	1.72–11.1
Short	9/245	0.72	0.32–1.61	3.20	1.13–9.00

[a]RR1: genetic relative risks, *Short* versus *Long* genotype, adjusted for age, gender, city and smoking.
[b]95% confidence interval.
[c]RR2: genetic and radiation-related risks, with reference to non-exposed *Long* genotype.
[d]Reference category.
[e]712 mGy: median dose in exposed sub-cohort members.

(30–50%) (31). The results suggest that the *EGFR* CA repeat number polymorphism may work as an indicator of individuals susceptible to lung cancer, specifically adenocarcinoma, in the Japanese population who have not been exposed to ionizing radiation. One limitation of this study is that no information about the *EGFR* mutation status of the cases was available. Population-based risk estimation of *EGFR*-mutated lung cancer for the CA repeat number polymorphism is therefore a goal of future research. Interestingly, the shorter CA repeat length has been reported to be associated with *EGFR* mutations among lung adenocarcinoma patients (23).

When looking at radiation dose effects on lung cancer risk, A-bomb survivors with the *Long* genotype were found to have a significant elevation of lung cancer risk that increased with increasing radiation dose, whereas the risk among those with the *Short* genotype did not change with radiation dose (Tables III and IV). As a result, the differences in risk between the *Long* and *Short* genotypes decreased with increasing radiation dose. Compared with the *Short* genotype, the *Long* genotype, presumably possessed by more than half of the Japanese population, is hypothesized to confer increased susceptibility to lung cancer after radiation exposure, although the baseline risk at no radiation dose is lower than that with the *Short* genotype. Our findings imply that individuals with the *Long* genotype, who are genetically at low risk of lung cancer when they are not exposed to radiation, may have to be more cautious about medical or occupational radiation exposure to minimize the cancer risk, which would otherwise show an elevation due to their high sensitivity to radiation.

We attempted two different methods of summarizing genotypes: summing CA repeat numbers of two alleles in each individual (resulting in *Long* or *Short* genotype) or combining allele-specific genotypes (resulting in *long/long*, *long/short* or *short/short* genotype). Although both methods produced similar results (Tables II–IV compared with supplementary Tables SI–SIII are available at *Carcinogenesis* Online), results from the latter method seem to be less clear, being in part due to an insufficient number of cases, especially of the *short/short* genotype. This also suggests that both alleles may combine to contribute to the risk of lung cancer, not in an allele-specific way (i.e. no preference for a contributory allele). In addition, analyses in this study were based on the weighted skin dose as an approximation for air dose. There were no substantial differences in the relative risks obtained using skin dose and lung dose, as shown by RR2 (2.45, 95% CI: 1.22–4.92, Table III) for *Short* genotype in the highest skin dose group compared with RR2 (2.45, 95% CI: 1.25–4.83) in the highest lung dose group.

Although the precise mechanism linking the CA repeat polymorphism and lung cancer risk remains to be elucidated, the shorter CA repeat length has been reported to be associated with increased *EGFR* transcription activity—supposedly by alteration in the repressor protein binding property (21,22,32)—and also with an increased *EGFR* mutation rate (23). Thus, the increased risk for the *Short* genotype observed in this study for non-exposed individuals may be in part ascribed to the inherent high EGFR production ability. Furthermore, it is probably that there is an undefined transcriptional mechanism that contributes to the more efficient EGFR production in individuals with the *Long* genotype than with the *Short* genotype as radiation dose increases, which results in an elevated lung cancer risk for the *Long* genotype with radiation dose. Further work, including *in vitro* studies, is required to establish the mechanistic link between the CA repeat polymorphism, EGFR production and radiation exposure in lung carcinogenesis.

Supplementary material

Supplementary Tables I–III can be found at http://carcin.oxfordjournals.org/

Funding

RERF Research Protocol 4-04; Ground-based Research Program for Space Utilization, Japan Space Forum; Grant-in-Aid for Scientific Research, Japanese Ministry of Education, Culture, Sports, Science and Technology (21390199 and 20014032); Grant-in-Aid for the 3rd-term Comprehensive 10-year Strategy for Cancer Control, Japanese Ministry of Health, Labour and Welfare (H21-04).

Acknowledgements

The Radiation Effects Research Foundation, Hiroshima and Nagasaki, Japan, is a private non-profit foundation funded by the Japanese Ministry of Health, Labour and Welfare and the US Department of Energy, the latter in part through the National Academy of Sciences.

Conflict of Interest Statement: None declared.

References

1. Jemal,A. *et al.* (2008) Cancer statistics, 2008. *CA Cancer J. Clin.*, **58**, 71–96.
2. Shields,P.G. *et al.* (2000) Cancer risk and low-penetrance susceptibility genes in gene-environment interactions. *J. Clin. Oncol.*, **18**, 2309–2315.
3. Schwartz,A.G. *et al.* (2007) The molecular epidemiology of lung cancer. *Carcinogenesis*, **28**, 507–518.
4. Sun,S. *et al.* (2007) Lung cancer in never smokers—a different disease. *Nat. Rev. Cancer*, **7**, 778–790.
5. Krewski,D. *et al.* (2006) A combined analysis of North American case-control studies of residential radon and lung cancer. *J. Toxicol. Environ. Health A*, **69**, 533–597.
6. Menzler,S. *et al.* (2008) Population attributable fraction for lung cancer due to residential radon in Switzerland and Germany. *Health Phys.*, **95**, 179–189.
7. Preston,D.L. *et al.* (2007) Solid cancer incidence in atomic bomb survivors: 1958-1998. *Radiat. Res.*, **168**, 1–64.
8. Kyoizumi,S. *et al.* (2005) Individual variation of somatic gene mutability in relation to cancer susceptibility: prospective study on erythrocyte glycophorin a gene mutations of atomic bomb survivors. *Cancer Res.*, **65**, 5462–5469.
9. Herbst,R.S. *et al.* (2008) Lung cancer. *N. Engl. J. Med.*, **359**, 1367–1380.
10. Sozzi,G. *et al.* (1991) Cytogenetic abnormalities and overexpression of receptors for growth factors in normal bronchial epithelium and tumor samples of lung cancer patients. *Cancer Res.*, **51**, 400–404.
11. Shigematsu,H. *et al.* (2006) Somatic mutations of epidermal growth factor receptor signaling pathway in lung cancers. *Int. J. Cancer*, **118**, 257–262.
12. Liang,K. *et al.* (2003) The epidermal growth factor receptor mediates radioresistance. *Int. J. Radiat. Oncol. Biol. Phys.*, **57**, 246–254.
13. Brattstrom,D. *et al.* (2004) HER-2, EGFR, COX-2 expression status correlated to microvessel density and survival in resected non-small cell lung cancer. *Acta Oncol.*, **43**, 80–86.
14. Yacoub,A. *et al.* (2006) Radiotherapy-induced signal transduction. *Endocr. Relat. Cancer*, **13** (suppl. 1), S99–S114.

15. Rodemann,H.P. *et al.* (2007) Radiation-induced EGFR-signaling and control of DNA-damage repair. *Int. J. Radiat. Biol.*, **83**, 781–791.
16. Liu,W. *et al.* (2005) A functional common polymorphism in a Sp1 recognition site of the epidermal growth factor receptor gene promoter. *Cancer Res.*, **65**, 46–53.
17. Chi,D.D. *et al.* (1992) Two chromosome 7 dinucleotide repeat polymorphisms at gene loci epidermal growth factor receptor (EGFR) and pro alpha 2 (I) collagen (COL1A2). *Hum. Mol. Genet.*, **1**, 135.
18. Nomura,M. *et al.* (2007) Polymorphisms, mutations, and amplification of the EGFR gene in non-small cell lung cancers. *PLoS Med.*, **4**, e125.
19. Liu,W. *et al.* (2003) Interethnic difference in the allelic distribution of human epidermal growth factor receptor intron 1 polymorphism. *Clin. Cancer Res.*, **9**, 1009–12.
20. Buerger,H. *et al.* (2004) Allelic length of a CA dinucleotide repeat in the egfr gene correlates with the frequency of amplifications of this sequence—first results of an inter-ethnic breast cancer study. *J. Pathol.*, **203**, 545–550.
21. Gebhardt,F. *et al.* (1999) Modulation of epidermal growth factor receptor gene transcription by a polymorphic dinucleotide repeat in intron 1. *J. Biol. Chem.*, **274**, 13176–13180.
22. Buerger,H. *et al.* (2000) Length and loss of heterozygosity of an intron 1 polymorphic sequence of egfr is related to cytogenetic alterations and epithelial growth factor receptor expression. *Cancer Res.*, **60**, 854–857.
23. Sueoka-Aragane,N. *et al.* (2008) Exon 19 of EGFR mutation in relation to the CA-repeat polymorphism in intron 1. *Cancer Sci.*, **99**, 1180–1187.
24. Lee,S.J. *et al.* (2007) No association between dinucleotide repeat polymorphism in intron 1 of the epidermal growth factor receptor gene EGFR and risk of lung cancer. *Cancer Genet. Cytogenet.*, **172**, 29–32.
25. Zhang,W. *et al.* (2007) Association of the EGFR intron 1 CA repeat length with lung cancer risk. *Mol. Carcinog.*, **46**, 372–380.
26. Yamada,M. *et al.* (2004) Noncancer disease incidence in atomic bomb survivors, 1958-1998. *Radiat. Res.*, **161**, 622–632.
27. Sato,T. (1994) Risk ratio estimation in case-cohort studies. *Environ. Health Perspect.*, **102** (suppl. 8), 53–56.
28. Therneau,T.M. *et al.* (1999) Computing the Cox model for case cohort designs. *Lifetime Data Anal.*, **5**, 99–112.
29. Cullings,H.M. *et al.* (2006) Dose estimation for atomic bomb survivor studies: its evolution and present status. *Radiat. Res.*, **166**, 219–254.
30. Amador,M.L. *et al.* (2004) An epidermal growth factor receptor intron 1 polymorphism mediates response to epidermal growth factor receptor inhibitors. *Cancer Res.*, **64**, 9139–9143.
31. Sequist,L.V. *et al.* (2007) Molecular predictors of response to epidermal growth factor receptor antagonists in non-small-cell lung cancer. *J. Clin. Oncol.*, **25**, 587–595.
32. Brandt,B. *et al.* (2006) Mechanisms of egfr gene transcription modulation: relationship to cancer risk and therapy response. *Clin. Cancer Res.*, **12**, 7252–7260.

Received September 3, 2009; revised September 3, 2009; accepted October 8, 2009

Carcinogenesis vol.30 no.12 pp.2042–2046, 2009
doi:10.1093/carcin/bgp257
Advance Access publication October 25, 2009

Common genetic variation in *IGF1*, *IGFBP1* and *IGFBP3* and ovarian cancer risk

Kathryn L.Terry[1,2,*], Shelley S.Tworoger[2,3], Margaret A.Gates[2,3], Daniel W.Cramer[1,2] and Susan E.Hankinson[2,3]

[1]Obstetrics and Gynecology Epidemiology Center, Department of Obstetrics and Gynecology, Brigham and Women's Hospital, 221 Longwood Avenue, Boston, MA 02115, USA, [2]Department of Epidemiology, Harvard School of Public Health, Boston, MA 02115, USA and [3]Channing Laboratory, Department of Medicine, Brigham and Women's Hospital and Harvard Medical School, Boston, MA 02115, USA

*To whom correspondence should be addressed. Tel: +617 732 4895; Fax: +617 732 4899;
Email: kterry@partners.org

Insulin-like growth factor (IGF) 1 and its binding proteins foster cellular proliferation and inhibit apoptosis. *In vitro* studies show that IGF1 increases ovarian cell growth and invasive potential, suggesting a role for the IGF1 pathway in ovarian cancer etiology. We evaluated genetic variation in the *IGF1*, *IGFBP1* and *IGFBP3* genes in relation to ovarian cancer risk by genotyping 29 haplotype-tagging single nucleotide polymorphisms in 1173 cases and 1201 controls from the New England Case–Control (NECC) study and 296 cases and 854 controls from the Nurses' Health Study (NHS). The association of haplotypes and single nucleotide polymorphisms (SNPs) with ovarian cancer was estimated using unconditional (NECC) and conditional (NHS) logistic regression. Additionally, we evaluated the association of SNPs with IGF1, IGF-binding protein (IGFBP) 3 and IGFBP2 plasma levels (n = 380 NHS controls). Our data suggest a decreased risk for women carrying haplotype 2C of the *IGF1* gene [odds ratios (ORs) = 0.82, 95% confidence intervals (CIs) = 0.69–0.98] and an increased risk for women carrying haplotype 1D (OR = 1.41, 95% CI = 1.03–1.94) or 2D (OR = 1.20, 95% CI = 1.01–1.41) in the binding proteins. When evaluated individually, three SNPs in the IGFBPs (rs10228265, rs4988515 and rs2270628) were associated with increased ovarian cancer risk, and several *IGF1* (rs11111285, rs1996656 and rs1019731) and *IGFBP3* (rs2270628, rs2854746 and rs2854744) SNPs were significantly associated with IGF1, IGFBP3 and IGFBP2 plasma levels. Some haplotypes and SNPs in the IGF pathway genes may be associated with ovarian cancer risk; however, these results need to be confirmed. Of particular interest was the *IGFBP3* SNP rs2270628, which was associated with both increased IGF1 plasma levels and higher ovarian cancer risk.

Introduction

Insulin-like growth factor (IGF) 1 and its binding proteins foster cellular proliferation and inhibit apoptosis. Biologic evidence from *in vitro* studies shows that IGF1 increases ovarian cell growth and invasive potential, suggesting a role for the IGF1 pathway in ovarian cancer etiology (1–4). Epidemiologic data regarding plasma IGF1 levels and ovarian cancer risk are conflicting. Two prospective studies observed that plasma IGF1 levels are associated with an increased risk of ovarian cancer among younger women (5,6), whereas data from the Nurses' Health Study (NHS) suggested that plasma IGF1 levels may be inversely associated with ovarian cancer risk (19). With respect to IGF-binding proteins (IGFBPs), the prospective studies agree that there are no clear associations of IGFBP3 and IGFBP2 with ovarian cancer risk (5–8).

Abbreviations: CIs, confidence intervals; FPRP, false-positive report probability; htSNPs, haplotype-tagging single nucleotide polymorphisms; HWE, Hardy–Weinberg Equilibrium; IGF, insulin-like growth factor; IGFBP, IGF-binding protein; NECC, New England Case–Control; NHS, Nurses' Health Study; ORs, odds ratios; SNPs, single nucleotide polymorphisms.

Given that genetic variation in the *IGF1*, *IGFBP1* and *IGFBP3* genes are likely to influence plasma levels of IGF1 (9) and its binding proteins and that genetic variation may be a better measure of exposure over a lifetime than a single plasma measurement, we examined whether genetic variation in *IGF1*, *IGFBP1* and *IGFBP3* was associated with ovarian cancer risk in two large population-based studies [New England Case–Control (NECC) study and NHS].

Materials and methods

Study population

New England Case–Control study. Data and specimens from this NECC study of ovarian cancer come from two enrollment phases (phase 1: 1992–1997 and phase 2: 1998–2002) corresponding to two funding periods. Details regarding case and control enrollment are described elsewhere (10). Briefly, 2347 women residing in eastern Massachusetts or New Hampshire with a diagnosis of incident ovarian cancer were identified through hospital tumor boards and statewide cancer registries. Of these women, 1845 were eligible and 1306 (71% of the eligible cases, 1231 epithelial cases) agreed to participate. Controls were identified through a combination of random digit dialing, drivers' license lists and town resident lists. In the first phase, 421 (72%) of the eligible women identified through random digit dialing agreed to participate and 102 (51%) of the eligible women identified through town resident lists agreed to participate. In the second phase, 1843 potential controls were identified, 1267 were eligible, 546 declined to participate by phone or by mail via an 'opt-out' postcard and 721 (57%) were enrolled. Controls were frequency matched to cases on age and state of residence.

All study participants were interviewed at the time of enrollment about known and suspected ovarian cancer risk factors. To avoid the possible impact of preclinical disease on exposure status, cases were asked about exposures that occurred at least 1 year before diagnosis and controls were asked about exposures that occurred >1 year before the interview date. More than 95% of the participants provided a blood specimen that was separated into plasma, red blood cell and buffy coat components and stored in −80°C freezers.

Nurses' Health Study. The NHS cohort was established in 1976 among 121 700 US female registered nurses aged 30–55 years. Women completed an initial questionnaire and have been followed biennially by questionnaire to update exposure status and disease diagnoses.

In 1989–1990, 32 826 participants submitted a blood sample; details of the collection are described elsewhere (11). All samples have been stored in liquid nitrogen freezers since collection. Follow-up of the NHS blood study cohort was 96.1% in 2006. In 2001–2004, 33 040 additional women provided a buccal cell specimen using a mouthwash protocol; follow-up was 99% through 2006. We extracted DNA from each buccal cell specimen within 1 week of receipt using Qiagen DNA Extraction Kit (Qiagen, Valencia, CA) and stored the DNA at −80°C. These studies were approved by the Committee on the Use of Human Subjects in Research at the Brigham and Women's Hospital.

NHS nested case–control study. We collected information on new diagnoses of ovarian cancer and confirmed each diagnosis using methods described previously (12). For this analysis, we included all cases with a DNA specimen submitted prior to diagnosis (incident cases) plus cases who submitted a DNA specimen within 4 years after diagnosis (prevalent cases). The incident and prevalent cases were similar with respect to stage, histology and survival time (13). All cases were diagnosed prior to 1 June 2004 and had no history of a prior cancer, other than non-melanoma skin cancer.

We randomly selected three controls per case from the study participants with DNA available, no prior bilateral oophorectomy and no history of cancer, other than non-melanoma skin cancer, at the time of case diagnosis. We excluded 27 controls from the analysis due to unavailability of genotyping data (n = 25) or because the participant was later diagnosed with ovarian cancer and was included in the analysis as a case (n = 2). Cases and controls were matched on age, menopausal status at baseline and diagnosis, month of blood collection, time of day of blood draw, fasting status and postmenopausal hormone use at blood draw.

Genotyping methods

We selected *IGF1*, *IGFBP1* and *IGFBP3* haplotype-tagging single nucleotide polymorphisms (htSNPs) identified by the Breast and Prostate Cancer Cohort Consortium (http://ccnt.hsc.usc.edu/MECGenetics/) (9,12,14–16). Their method of htSNP selection has been described elsewhere (17). Briefly, single

Changes of ROS during a Two-day Ultra-marathon Race

Authors

N. Hattori[1], T. Hayashi[2], K. Nakachi[2], H. Ichikawa[3], C. Goto[4], Y. Tokudome[5], K. Kuriki[6], H. Hoshino[7], K. Shibata[8], N. Yamada[9], M. Tokudome[10], S. Suzuki[3], T. Nagaya[1], M. Kobayashi[11], S. Tokudome[3]

Affiliations

Affiliation addresses are listed at the end of the article

Key words
- reactive oxygen species
- ultra-marathon
- oxidative stress
- physical performance

Abstract

To assess oxidative stress (OS) induced by endurance exercise, concentrations of serum reactive oxygen species (ROS) were determined in 70 Japanese male amateur runners completing a two-day ultra-marathon race. Serum ROS levels were analyzed at three time points: before the race (baseline), after the 1st day race (mid-race), and after the 2nd day race (goal) (post-race). The means (SE) of ROS were 151.4(3.7) (U. CARR.), 168.7(4.4), and 156.8(4.4), respectively. Significant positive trends were noted between age and serum ROS concentrations at the three race points ($p<0.05$ for all). After adjusting for age, BMI and average monthly running distance, the baseline serum ROS concentrations were positively associated with completion times of the first-day race, in particular ($p<0.05$), suggesting that the concentrations may predict physical performance. The ROS production increased at mid-race ($p<0.05$), but the levels returned to baseline levels at post-race, indicating that an antioxidant defense system may develop post-race to reduce OS.

accepted after revision
November 28, 2008

Bibliography
DOI 10.1055/s-0028-1112144
Published online:
February 6, 2009
Int J Sports Med 2009; 30:
426–429 © Georg Thieme
Verlag KG Stuttgart · New York
ISSN 0172-4622

Correspondence
S. Tokudome
Public Health
Nagoya City University
Graduate School of Medical
Sciences
Kawasumi-1
Mizuho-cho, Mizuho-ku
467-8601 Nagoya
Japan
Tel.: +81/52/853 81 74
Fax: +81/52/842 38 30
tokudome@
med.nagoya-cu.ac.jp

Introduction

Moderate/vigorous physical exercise results in 10–20 times more oxygen uptake than the resting condition, and electron fluxes into the mitochondria of skeletal muscles are enhanced 100–200 times, which inevitably produce reactive oxygen species (ROS). Strenuous physical exercise subsequently induces ischemia-reperfusion injury, inflammation, and muscle damage in proportion to the intensity of exercise and oxygen consumed [3,26,27]. Although many ROS exist, hydroxy-radical (·OH), alkoxy-radical (·OR) and peroxy-radical (·OOR) are highly detrimental and responsible for oxidative stress (OS) on DNAs [33], cells, and cell membranes [25]. Moreover, they have been implicated in aging [13,16] as well as with the onset/progression of cerebro- and cardio-vascular disease, neuromuscular disease, autoimmune disease, and cancer [30,37,40].

Long-term running like an ultra-marathon race imposes OS on cardio-respiratory functions and skeletal muscles [35]. OS yielded by endurance exercise inevitably contributes to muscular damage, lowers physical performance, and induces fatigue due to destruction of cellular macromolecules such as lipids, proteins, and nucleic acids during physical exercise [21,25,32]. However, regular physical exercise and endurance training confer protection against ROS and improve antioxidant defenses by upregulation of responsible gene expression [20,29,32,33,41]. Regular physical activity has therefore been recommended for health promotion [34,39]. In fact, we formerly noted that levels of urinary 8-hydroxydeoxyguanosine (8-OHdG), a marker of oxidative DNA damage, rose after the 1st day running 40 km, but returned to baseline after the 2nd day running 90 km in non-professional Japanese athletes completing a two-day ultra-marathon race. This suggested that prolonged running causes oxidative DNA damage, but antioxidant repair systems are subsequently induced to protect against OS [28].

We here investigated changes of serum ROS concentrations using the D-Roms test [2,4], which directly assesses total ROS, based on the ability of transition metals to catalyze ·OH ·OR, and ·OOR. We also examined correlations between the serum ROS levels and age, alcohol use, smoking, or average monthly running distance, along with any association between baseline serum ROS concentrations and running performance in men finishing the two-day ultra-marathon race.

Table 1 Serum ROS concentrations at baseline and completion times of two race points according to age.

	Age (years)			
	-44	45–54	55-	
	n=23	n=31	n=16	
serum ROS (U. CARR.)	140.2±3.5*	155.4±3.8	161.7±3.5	<0.005**
completion time of 1st-day race (min)	286.5±11.2	303.8±8.5	299.5±11.9	
completion time of 2nd-day race (min)	747.4±28.6	776.7±20.3	791.6±28.2	
total completion time (min)	1033.8±38.6	1080.5±30	1091±38.9	

*Mean±SE

**p value for regression coefficient

Subjects and Methods

Ultra-marathon race

The ultra-marathon race, as described elsewhere [42], was held in Gifu Prefecture, Japan, July 27–28, 2002. In brief, the race involved running 130 km over two days. The weather was partly cloudy, hot and sultry. On the first day, participants started at 11:00 a.m. and ran approximately 40 km within 6.5 h. At 3:30 a.m. on the second morning, they resumed the race to run about 90 km including climbing up to a mountain lake approximately 1100 m high, then returning to the starting point within 15.5 h.

Subjects and methods

Six weeks prior to the race, we administered a questionnaire by mail to all participants. Of them, 161 male runners agreed to participate in the study and gave written informed consent. The analysis was limited to 70 male runners who completed the entire two-day race. We obtained information on demographic anthropometric and lifestyle characteristics, including age, sex, height, weight, smoking and alcohol drinking habits, and average monthly running distance. No specific instructions, including meals and beverages, were given before or during the race.

Baseline blood samples at rest were collected approximately one-two hours before the first stage. Mid-race and post-race samples were obtained less than three-five minutes after the first stage and the final stage.

Serum ROS concentrations were determined by the D-Roms test, using the FRAS 3 (Diacron, Grosseto, Italy) developed by Alberti [1]. The test directly estimates serum ROS levels resulting in cells as a consequence of respiratory burst in the presence of irons acting as catalyzers. ROS react with the exact same number of alkylamines (N, N-diethyl-para-phenylendiamine) and develop a colored complex showing peak absorbance at 505 nm. The concentrations of the colored complex are directly proportional to the total serum ROS levels [17]. One Carratelli unit (U. CARR.) corresponds to 0.8 mg/L hydrogen peroxide. In brief, 20 µl serum and 1.2 ml buffered solution (R2 reagent) were mixed in a cuvette, and 20 µl chromogen substrate (R1 reagent) was added. After shaking to mix, the cuvette was centrifuged for 1 min at 37°C and incubated for 5 min at 37°C. Absorbance at 505 nm was monitored for 3 min. The coefficient of variation of ROS measurements was less than 4.3%.

The study protocol was approved by the Institutional Review Board of Nagoya City University Graduate School of Medical Sciences.

Statistical analysis

Mean values or prevalence of baseline characteristics, serum ROS concentrations, and completion times were calculated according to age group (≤44, 45–54, or ≥55). While the trends were probed by linear regression analysis, an analysis of variance (ANOVA) for repeated measures was adopted for comparison of the mean serum ROS levels at baseline, mid-race, and post-race. Tukey's post hoc multiple t-test was performed to examine differences in the least square means. Statistical significance was set at $p<0.05$.

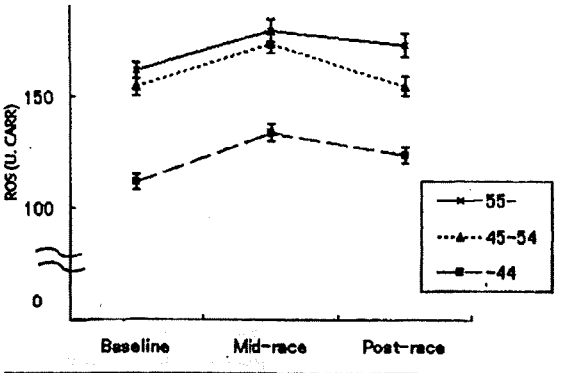

Age	n	Baseline	Mid-race	Post-race
55-	16	161.7±3.5	178.5±5.1*	172.9±5.3
45-54	31	154.4±3.8	173.3±4.3*	154.6±4.3§
-44	23	140.2±3.5	155.2±3.8**	148.5±3.6
All	70	151.4±3.7	168.7±4.4**	156.8±4.4§§

Fig. 1 Changes of serum ROS levels at baseline, mid-race and post-race according to age. Note: Mean±SE, ANOVA for repeated measures was adopted for comparison of the ROS values at baseline (1), mid-race (2) and post-race (3) along with Tukey's post hoc multiple t-test. +$p<0.05$ vs. baseline, ++$p<0.01$ vs. baseline, §$p<0.05$ vs. mid-race, §§$p<0.01$ vs. mid-race.

Results

In all age categories, BMI and percentage of smoking (0–6.5%) were much smaller than those of the general public [42], whereas alcohol consumption (60–75%) was greater (data not shown). Serum ROS levels at baseline were positively related to age ($p<0.005$) (● **Table 1**). Completion times were not significantly related to age, but were positively associated with BMI, and inversely related to average monthly running distance. On the other hand, serum ROS levels were not associated with average monthly running distance. After adjustment for age, BMI and average monthly running distance, baseline serum ROS concentrations were positively related to completion times, after the first-day goal, in particular.

Table 2 Matrices of Pearson's correlation coefficients among serum ROS concentrations, age, BMI, average monthly running distance and completion time.

		Age	BMI	Average monthly running distance	Completion time		
					1st day	2nd day	Total
serum ROS concentrations	baseline	0.33**	0.09	−0.04	0.34**	0.28*	0.30*
	mid-race	0.30*	0.09	0.11	0.16	0.14	0.15
	post-race	0.24*	0.08	−0.01	0.15	0.18	0.17
age			0.04	0.07	0.21	0.20	0.21
BMI				0.07	0.25*	0.27*	0.27*
average monthly running distance					−0.66***	−0.62***	−0.65***
completion time	1st day					0.84****	0.92****
	2nd day						0.98****
	total						
adjusted serum ROS concentrations[a)]	baseline				0.34*	0.23	0.28*

*p<0.05, **p<0.01, ***p<0.0001

a)Adjusted for age, BMI and average monthly running distance

Overall means(SE) of serum ROS levels at baseline, mid-race, and post-race were 151.4(3.7)(U. CARR.), 168.7(4.4), and 156.8(4.4), respectively. The age group-specific serum ROS concentrations at mid-race were universally higher than those at baseline (● **Fig. 1**), and the post-race levels returned to the baseline value. In particular, the group less than 45 years old had lower ROS levels at all race points (● **Table 2**).

Discussion

This is, to our knowledge, the first study of changes in serum ROS concentrations in ultra-marathon runners. Significantly higher serum ROS levels were demonstrated among older than younger runners. Age was not related to completion times; however, there were significant positive correlations between baseline serum ROS concentrations and completion times. Our study also showed apparent elevations of serum ROS levels after the first day running 40 km. However, the values subsequently returned to baseline after the second day running 90 km in spite of double the running distance.

Aging is a critical determining factor for OS [15,18,19,24,32]. Many studies have demonstrated a ROS theory of life span or aging associated with mitochondrial ROS production [25,36], cumulative damage to DNA [23,33], inflammation [32,43] and lipid peroxidation in aged tissues such as skeletal muscle [9,10]. As reported previously, physical exercise may compensate for the elevation in the OS associated with aging [12,38]. In the present study, serum ROS concentrations of all physically trained runners were apparently lower than in their healthy counterparts (250–300 U. CARR.) [2,4]. Serum ROS concentrations adjusted for age, BMI and average monthly running distance were related to completion times, after the first day race, in particular, indicating that serum ROS levels at baseline may predict physical performance, which is compatible with the observations that serum ROS concentrations appear to be associated with anti-oxidant defenses. The runners were exposed to a large quantity of oxygen, and the inevitable increased ROS generation during exercise serves as messenger in exercise-induced adaptive gene expression [7,32]. Elite marathon runners usually have higher maximum oxygen intake (VO_2max) values [6,11,14]. As is the case for VO_2max, serum ROS concentrations may be a key factor in the performance of endurance exercises, including marathon and ultra-marathon running. This may corroborate observations that ROS generation effectively results in lower baseline ROS concentrations, increased activity of antioxidant and damage repair enzymes, and lower oxidative damage levels [31,32]. However, we failed to detect an inverse association between the average monthly running distance and serum ROS levels, which may be partly due to the relatively narrow range of the average monthly running distance among the participants.

We previously observed that concentrations of urinary 8-OHdG elevated after the first stage and returned to baseline level after the second stage [28]. Similarly, we detected concordant changes in serum ROS concentrations in the present study, indicating that exercise-induced serum ROS were potentially attenuated by delayed upregulation in antioxidant gene expression and/or increased enzymatic activity [5,8,24]. Indeed, Kostaropoulos et al. [22] have noted higher catalase activity in long-distance runners than short-distance runners. These observations suggested that prolonged exercise may upregulate an antioxidant defense system to cope with exercise-induced OS.

In conclusion, our study indicated that serum ROS concentrations are associated with age in ultra-marathon runners. Serum ROS levels at baseline appear to predict the physical performance of ultra-marathon runners. We observed that prolonged running increased the serum ROS concentrations after the first day, but returned to baseline after the second day, which may well be due to upregulation of an anti-oxidation system.

Acknowledgements

This study was supported, in part, by a Grant-in-Aid from the Ministry of Education, Culture, Sports, Science, and Technology, Japan. We appreciate the runners having willingly participated in our study and the chairman and organizing committee of the Maranic race. We thank Ms. Fujii, T., Ms. Kubo, Y., Ms. Nakanishi, N., Ms. Ito, Y., Ms. Higuchi, K., and Ms. Watanabe, M. for their technical assistance.

Affiliations

[1] Public Health, Nagoya City University Graduate School of Medical Sciences, Nagoya, Japan

[2] Department of Radiobiology/Molecular Epidemiology, Radiation Effects Research Foundation, Hiroshima, Japan

[3] Department of Health Promotion and Preventive Medicine, Nagoya City University Graduate School of Medical Sciences, Nagoya, Japan

[4] Department of Health and Nutrition, Nagoya Bunri University, Inazawa, Japan
[5] School of Nutritional Sciences, Nagoya University of Arts and Sciences, Nisshin, Japan
[6] Department of Epidemiology and Prevention, Aichi Cancer Center Research Institute, Nagoya, Japan
[7] Department of Health Promotion, Aichi Bunkyo Women's College, Inazawa, Japan
[8] Department of Health Promotion, Kasugai Health Maintenance Center, Kasugai, Japan
[9] Department of Nutrition, Tenshi College, Sapporo, Japan
[10] Medical Center, Yokohama City University, Yokohama, Japan
[11] Department of Musculoskeletal Medicine, Nagoya City University Graduate School of Medical Sciences, Nagoya, Japan

References

1 *Alberti A, Bolognini L, Macciantelli D, Caratelli M.* The radical cation of N, N-diethyl-para-phenylendiamine: a possible indicator of oxidative stress in biological samples. Res Chem Intermed 1999; 26: 253–267
2 *Cesarone MR, Belcaro G, Carratelli M, Cornelli U, Sanctis MT De, Incandela L, Barsotti A, Terranova R, Nicolaides A.* A simple test to monitor oxidative stress. Int Angiol 1999; 18: 127–130
3 *Child RB, Wilkinson DM, Fallowfield JL, Donnelly AE.* Elevated serum antioxidant capacity and plasma malondialdehyde concentration in response to a simulated half-marathon run. Med Sci Sports Exerc 1998; 30: 1603–1607
4 *Cornelli U, Terranova R, Luca S, Cornelli M, Alberti A.* Bioavailability and antioxidant activity of some food supplements in men and women using the D-Roms test as a marker of oxidative stress. J Nutr 2001; 131: 3208–3211
5 *Criswell D, Powers S, Dodd S, Lawler J, Edwards W, Renshler K, Grinton S.* High intensity training-induced changes in skeletal muscle antioxidant enzyme activity. Med Sci Sports Exerc 1993; 25: 1135–1140
6 *Davies CT, Thompson MW.* Aerobic performance of female marathon and male ultramarathon athletes. Eur J Appl Physiol 1979; 41: 233–245
7 *Davies KJ, Quintanilla AT, Brooks GA, Packer L.* Free radicals and tissue damage produced by exercise. Biochem Biophys Res Commun 1982; 107: 1198–1205
8 *Elosua R, Molina L, Fito M, Arquer A, Sanchez-Quesada JL, Covas MI, Ordonez-Llanos J, Marrugat J.* Response of oxidative stress biomarkers to a 16-week aerobic physical activity program, and to acute physical activity, in healthy young men and women. Atherosclerosis 2003; 167: 327–334
9 *Evans W.* Functional and metabolic consequences of sarcopenia. J Nutr 1997; 127: 998S–1003S
10 *Evans WJ, Campbell WW.* Sarcopenia and age-related changes in body composition and functional capacity. J Nutr 1993; 123: 465–468
11 *Farrell PA, Wilmore JH, Coyle EF, Billing JE, Costill DL.* Plasma lactate accumulation and distance running performance. Med Sci Sports 1979; 11: 338–344
12 *Fatouros IG, Jamurtas AZ, Villiotou V, Pouliopoulou S, Fotinakis P, Taxildaris K, Deliconstantinos G.* Oxidative stress responses in older men during endurance training and detraining. Med Sci Sports Exerc 2004; 36: 2065–2072
13 *Flora SJ.* Role of free radicals and antioxidants in health and disease. Cell Mol Biol (Noisy-le-grand) 2007; 53: 1–2
14 *Hagan RD, Smith MG, Gettman LR.* Marathon performance in relation to maximal aerobic power and training indices. Med Sci Sports Exerc 1981; 13: 185–189
15 *Hagihara M, Nishigaki I, Maseki M, Yagi K.* Age-dependent changes in lipid peroxide levels in the lipoprotein fractions of human serum. J Gerontol 1984; 39: 269–272
16 *Halliwell B.* Oxidants and human disease: some new concepts. Faseb J 1987; 1: 358–364
17 *Hayashi I, Morishita Y, Imai K, Nakamura M, Nakachi K, Hayashi T.* High-throughput spectrophotometric assay of reactive oxygen species in serum. Mutat Res 2007; 631: 55–61
18 *Honda Y, Honda S.* Oxidative stress and life span determination in the nematode Caenorhabditis elegans. Ann N Y Acad Sci 2002; 959: 466–474
19 *Ji LL.* Antioxidant enzyme response to exercise and aging. Med Sci Sports Exerc 1993; 25: 225–231
20 *Knez WL, Jenkins DG, Coombes JS.* Oxidative stress in half and full Ironman triathletes. Med Sci Sports Exerc 2007; 39: 283–288
21 *Konig D, Wagner KH, Elmadfa I, Berg A.* Exercise and oxidative stress: significance of antioxidants with reference to inflammatory, muscular, and systemic stress. Exerc Immunol Rev 2001; 7: 108–133
22 *Kostaropoulos IA, Nikolaidis MG, Jamurtas AZ, Ikonomou GV, Makrygiannis V, Papadopoulos G, Kouretas D.* Comparison of the blood redox status between long-distance and short-distance runners. Physiol Res 2006; 55: 611–616
23 *Lee BM, Kwack SJ, Kim HS.* Age-related changes in oxidative DNA damage and benzo(a)pyrene diolepoxide-I (BPDE-I)-DNA adduct levels in human stomach. Toxicol Environ Health A 2005; 68: 1599–1610
24 *Leeuwenburgh C, Fiebig R, Chandwaney R, Ji LL.* Aging and exercise training in skeletal muscle: responses of glutathione and antioxidant enzyme systems. Am J Physiol 1994; 267: R439–445
25 *Leeuwenburgh C, Heinecke JW.* Oxidative stress and antioxidants in exercise. Curr Med Chem 2001; 8: 829–838
26 *Mastaloudis A, Morrow J, Hopkins D, Devaraj S, Traber M.* Antioxidant supplementation prevents exercise-induced lipid peroxidation, but not inflammation, in ultramarathon runners. Free Radic Biol Med 2004; 36: 1329–1341
27 *Mastaloudis A, Traber MG, Carstensen K, Widrick JJ.* Antioxidants did not prevent muscle damage in response to an ultramarathon run. Med Sci Sports Exerc 2006; 38: 72–80
28 *Miyata M, Kasai H, Kawai K, Yamada N, Tokudome M, Ichikawa H, Goto C, Tokudome Y, Kuriki K, Hoshino H, Shibata K, Suzuki S, Kobayashi M, Goto H, Ikeda M, Otsuka T, Tokudome S.* Changes of urinary 8-hydroxydeoxyguanosine levels during a two-day ultramarathon race period in Japanese non-professional runners. Int J Sports Med 2008; 29: 27–33
29 *Miyazaki H, Oh-ishi S, Ookawara T, Kizaki T, Toshinai K, Ha S, Haga S, Ji LL, Ohno H.* Strenuous endurance training in humans reduces oxidative stress following exhausting exercise. Eur J Appl Physiol 2001; 84: 1–6
30 *Papatheodorou L, Weiss N.* Vascular oxidant stress and inflammation in hyperhomocysteinemia. Antioxid Redox Signal 2007; 9: 1941–1958
31 *Radak Z, Chung HY, Goto S.* Exercise and hormesis: oxidative stress-related adaptation for successful aging. Biogerontology 2005; 6: 71–75
32 *Radak Z, Chung HY, Koltai E, Taylor AW, Goto S.* Exercise, oxidative stress and hormesis. Ageing Res Rev 2008; 7: 34–42
33 *Radak Z, Pucsuk J, Boros S, Josfai L, Taylor AW.* Changes in urine 8-hydroxydeoxyguanosine levels of super-marathon runners during a four-day race period. Life Sci 2000; 66: 1763–1767
34 *Reinehr T, Sousa G de, Toschke AM, Andler W.* Long-term follow-up of cardiovascular disease risk factors in children after an obesity intervention. Am J Clin Nutr 2006; 84: 490–496
35 *Sanchez LD, Corwell B, Berkoff D.* Medical problems of marathon runners. Am J Emerg Med 2006; 24: 608–615
36 *Schriner SE, Linford NJ, Martin GM, Treuting P, Ogburn CE, Emond M, Coskun PE, Ladiges W, Wolf N, Remmen H Van, Wallace DC, Rabinovitch PS.* Extension of murine life span by overexpression of catalase targeted to mitochondria. Science 2005; 308: 1909–1911
37 *Selfried HE, Anderson DE, Fisher EI, Milner JA.* A review of the interaction among dietary antioxidants and reactive oxygen species. J Nutr Biochem 2007; 18: 567–579
38 *Sial S, Coggan AR, Hickner RC, Klein S.* Training-induced alterations in fat and carbohydrate metabolism during exercise in elderly subjects. Am J Physiol 1998; 274: E785–790
39 *Sims J, Hill K, Davidson S, Gunn J, Huang N.* A snapshot of the prevalence of physical activity amongst older, community dwelling people in Victoria, Australia: patterns across the 'young-old' and 'old-old'. BMC Geriatr 2007; 7: 4
40 *Singh U, Jialal I.* Oxidative stress and atherosclerosis. Pathophysiology 2006; 13: 129–142
41 *Taddei S, Galetta F, Virdis A, Ghiadoni L, Salvetti G, Franzoni F, Giusti C, Salvetti A.* Physical activity prevents age-related impairment in nitric oxide availability in elderly athletes. Circulation 2000; 101: 2896–2901
42 *Tokudome S, Kuriki K, Yamada N, Ichikawa H, Miyata M, Shibata K, Hoshino H, Tsuge S, Tokudome M, Goto C, Tokudome Y, Kobayashi M, Goto H, Suzuki S, Okamoto Y, Ikeda M, Sato Y.* Anthropometric, lifestyle and biomarker assessment of Japanese non-professional ultra-marathon runners. J Epidemiol 2004; 14: 161–167
43 *Yao H, Edirisinghe I, Yang SR, Rajendrasozhan S, Kode A, Caito S, Adenuga D, Rahman I.* Genetic ablation of NADPH oxidase enhances susceptibility to cigarette smoke-induced lung inflammation and emphysema in mice. Am J Pathol 2008; 172: 1222–1237

reprints from

Cellular Immunology

Cellular Immunology
Vol. 255, Issue 1-2, pp 61-68, 2009

Caspase-independent cell death without generation of reactive oxygen species in irradiated MOLT-4 human leukemia cells

by
Kengo Yoshida, Yoshiko Kubo, Yoichiro Kusunoki, Yukari Morishita, Hiroko Nagamura, Ikue Hayashi, Seishi Kyoizumi, Toshio Seyama, Kei Nakachi, Tomonori Hayashi

ELSEVIER

Elsevier
Radarweg 29
1043 NX Amsterdam
The Netherlands
Tel: +31 (0)20 485 3440
Fax: +31 (0)20 485 3280

Cellular Immunology 255 (2009) 61–68

Contents lists available at ScienceDirect

Cellular Immunology

journal homepage: www.elsevier.com/locate/ycimm

Caspase-independent cell death without generation of reactive oxygen species in irradiated MOLT-4 human leukemia cells

Kengo Yoshida [a], Yoshiko Kubo [a], Yoichiro Kusunoki [a], Yukari Morishita [a], Hiroko Nagamura [a], Ikue Hayashi [b], Seishi Kyoizumi [a,c], Toshio Seyama [d], Kei Nakachi [a], Tomonori Hayashi [a,*]

[a] Department of Radiobiology/Molecular Epidemiology, Radiation Effects Research Foundation, 5-2 Hijiyama Park, Minami-ku, Hiroshima 732-0815, Japan
[b] Central Research Laboratory, Hiroshima University Faculty of Dentistry, Hiroshima, Japan
[c] Faculty of Human Ecology, Yasuda Women's University, Hiroshima, Japan
[d] Faculty of Pharmaceutical Sciences, Yasuda Women's University, Hiroshima, Japan

ARTICLE INFO

Article history:
Received 5 September 2008
Accepted 23 October 2008
Available online 9 December 2008

Keywords:
Apoptosis
Caspase
Immune cells
Ionizing radiation
Necrosis
Reactive oxygen species

ABSTRACT

To improve our understanding of ionizing radiation effects on immune cells, we investigated steps leading to radiation-induced cell death in MOLT-4, a thymus-derived human leukemia cell. After exposure of MOLT-4 cells to 4 Gy of X-rays, irradiated cells sequentially showed increase in intracellular reactive oxygen species (ROS), decrease in mitochondrial membrane potential, and eventually apoptotic cell death. In the presence of the caspase inhibitor z-VAD-fmk, irradiated cells exhibited necrotic characteristics such as mitochondrial swelling instead of apoptosis. ROS generation was not detected during this necrotic cell death process. These results indicate that radiation-induced apoptosis in MOLT-4 cells requires elevation of intracellular ROS as well as activation of a series of caspases, whereas the cryptic necrosis program—which is independent of intracellular ROS generation and caspase activation—is activated when the apoptosis pathway is blocked.

1. Introduction

A single cell-death-inducing stimulus such as ionizing radiation seems to evoke multiple and discrete mechanisms of cell death, and the physiological condition of the cells may determine the eventual outcome—whether apoptosis or necrosis, or another type of cell death [1]. Apoptosis and necrosis reveal varying postmortem features based on morphology, molecular events, and metabolic variations [2]. Immune responses to these two types of cell death may also differ in the event of radiation exposure including cancer radiotherapy (i.e., immune suppression in apoptosis vs. potent immune responses and inflammation in necrosis). Thus, elucidation of the cell-death mechanisms is essential to an improved understanding of radiation effects on a host. Early intracellular responses to radiation such as the possible involvement of reactive oxygen species (ROS)[1] in the process of apoptosis and/or necrosis, may determine the fate of irradiated cells and will be of particular interest in prevention and treatment of radiation-induced insults.

Apoptotic cell death is an active, programmed process of cell dismantling, which occurs under normal physiological and pathological conditions. Apoptotic features include chromatin condensation and fragmentation, overall cell shrinkage, formation of condensed cell bodies (apoptotic bodies), and minor changes in the cytoplasmic organelles. The molecular pathways of apoptosis, in which a series of cysteine proteases known as caspases play a central role, have been extensively studied over the last decade [3–5], but the upstream initiating events of radiation-induced apoptosis as well as the roles of mitochondria and ROS in these pathways remain to be elucidated [6].

Necrosis has thus far been considered passive and accidental cell death caused by extreme environmental perturbation, and characterized by plasma membrane rupture and swelling of the cytoplasmic organelles, particularly mitochondria. However, our current knowledge of what happens in the molecular pathways of radiation-induced necrosis is very limited. Recent studies using various cell types have shown that blockage of the apoptosis pathways failed to prevent cell death and instead led to necrotic cell death, which implies that necrosis is a physiologically alternative process of cellular dismantling under particular conditions [7–9].

Therefore, we investigated radiation-induced intracellular events, particularly ROS generation, to their conclusion in apoptosis or necrosis, using MOLT-4 cells with or without a caspase inhibitor z-VAD-fmk. Our results show that a 4 Gy X-ray irradiation mainly induced apoptotic cell death in MOLT-4 cells, but resulted in necrotic cell death in the presence of z-VAD-fmk. Moreover, generation of intracellular ROS was observed during the apoptotic

* Corresponding author. Fax: +81 82 261 3170.
E-mail address: tomo@rerf.or.jp (T. Hayashi).

[1] *Abbreviations used:* PI, propidium iodide; ROS, reactive oxygen species; z-VAD-fmk, *N*-benzyloxycarbonyl-Val-Ala-Asp-fluoromethylketone.

0008-8749/$ - see front matter © 2008 Elsevier Inc. All rights reserved.
doi:10.1016/j.cellimm.2008.10.006

process of irradiated MOLT-4 cells but not during the necrotic process of these cells pretreated with z-VAD-fmk: It is therefore possible that radiation may induce necrotic cell death through ROS-independent pathways.

2. Materials and methods

2.1. Cell culture

Human leukemia T cell line MOLT-4 [10] was obtained from the Japanese Cancer Resources Bank (Tokyo, Japan) and was grown in RPMI 1640 medium supplemented with 10% fetal calf serum (FCS), L-glutamine (2 mM), penicillin (100 units/ml), and streptomycin (100 μg/ml) in a 5% CO_2 humidified atmosphere. All experiments were performed with cells in the exponential growth phase.

2.2. Irradiation

Irradiation of cells was performed using an X-ray generator (Shimadzu HF-320; 220 kVp, 8 mA) with a 0.5 mm aluminum and 0.3 mm copper filter at a dose rate of approximately 0.8 Gy/min. Cells in the exponential growth phase were irradiated in RPMI 1640 with 10% FCS in a plastic dish at room temperature under normal oxygen tension.

2.3. Mitochondrial membrane potential and superoxide anions

To measure mitochondrial membrane potential ($\Delta\psi m$) and generation of the superoxide anions $O_2^{\cdot-}$, cells (5×10^5) were stained with 0.26 μM Rhodamine123 (Rh123; Molecular Probes, Eugene, OR) and 20 μM hydroethidine (HE; Molecular Probes), respectively, for 20 min at 37 °C [11–15]. Cells were washed once with phosphate buffered saline (PBS) containing 1% FCS, and then analyzed with a FACScan flow-cytometer (BD Biosciences, Franklin Lakes, NJ). To isolate certain cell fractions, cells were sorted using a FACS Vantage SE (BD Biosciences).

2.4. Phosphatidyl serine externalization and cell death

Externalization of the plasma membrane phosphatidyl serine, an early process of apoptosis, and cell death were assessed by measuring annexin V-FITC- and propidium iodide (PI)-stained cells, respectively, using a kit from MBL (Nagoya, Japan). After incubation in the reaction buffer (130 μl of binding buffer, 0.5 μl of annexin V-FITC, and 1.0 μl of PI) for 10 min, cells were analyzed using a FACScan flow-cytometer.

2.5. Catalytic activity of caspases

To suppress the activity of caspases, cells were pretreated with z-VAD-fmk (*N*-benzyloxycarbonyl-Val-Ala-Asp-fluoromethylketone; Peptide Institute, Osaka, Japan). Cells were suspended in the medium containing 100 μM z-VAD-fmk for 30 min prior to irradiation. Catalytic activity of a series of caspases was determined based on colorimetric assays. Cells (5×10^5) were lysed in lysis buffer (10 mM Tris–HCl, pH 7.4, 25 mM NaCl, 0.25% Triton X-100, 1 mM EDTA). The lysates were centrifuged at 16,000g at 4 °C for 30 min, and the supernatants were stored at −80 °C until analysis. Each supernatant (25 μg) was then incubated with 100 μl of caspase buffer (50 mM HEPES, pH 7.2, 100 mM NaCl, 1 mM EDTA, 10% sucrose, 0.1% CHAPS, 5 mM dithiothreitol) containing 100 μM substrates conjugated with 7-amino-4-methylcoumarin (Ac-VDVAD-AMC for caspase-2, Ac-DNLD-AMC for caspase-3, Ac-DEVD-AMC for caspase-3 and caspase-7, Ac-IETD-AMC for caspase-8, and Ac-LEHD-AMC for caspase-9) at 37 °C for 60 min. The release of 7-amino-4-methylcoumarin was measured using a spectrometer.

2.6. Cytochrome c release from mitochondria

Flow-cytometry was used to analyze cytochrome *c* release from mitochondria, as reported by Stahnke et al. [16]. Briefly, irradiated cells were fixed and permeabilized with 4% paraformaldehyde and 0.2% saponin for 20 min at 4 °C, and washed twice with Perm/Wash Buffer including fetal bovine serum, sodium azide, and saponin (BD Biosciences). Cells were incubated with 5 μg/ml mouse IgG to block nonspecific binding. Anti-cytochrome c antibody (1:20, clone 7H8.2C12, BD Biosciences) was then added, and cells were incubated at 4 °C for 20 min. Finally, cells were treated with goat anti-mouse IgG-FITC (1:20, Southern Biotech, Birmingham, AL) at 4 °C for 20 min and subjected to a FACScan flow-cytometer.

2.7. Transmission electron microscopy

Prefixation was performed with 2% glutaraldehyde in 100 mM cacodylate buffer, followed by washing in 100 mM cacodylate buffer overnight and subsequent postfixation with 2% osmium tetroxide in distilled water for 3 h. Cells were then dehydrated through a graded series of ethanol before being embedded in gelatin capsule with epoxy resin. Samples were sectioned into ultrathins (70–80 nm) using a LKB-8800 ultramicrotome (LKB, Bromma, Sweden), stained with 2% uranyl acetate in distilled water for 10 min and with lead staining solution for 5 min, and then examined using a JEM-2000EX (JEOL, Tokyo, Japan).

3. Results

3.1. Radiation-induced apoptotic cell death of MOLT-4 is characterized by decrease in mitochondrial membrane potential along with increase in intracellular ROS

Since a number of previous studies showed the crucial roles of mitochondria and ROS generation during apoptotic cell death by various stimuli [17–19], we first examined levels of mitochondrial membrane potential ($\Delta\psi m$) and intracellular superoxide anions (ROS) in X-ray-irradiated MOLT-4 cells. At 16 h after a 4 Gy irradiation, membrane potentials of irradiated cells had significantly decreased compared with those in unirradiated cells (Fig. 1A), while most irradiated cells showed elevated intracellular ROS (Fig. 1B). The irradiated MOLT-4 cells also exhibited several apoptotic features, including externalization of plasma membrane phosphatidyl serine (data not shown) and retention of normal mitochondrial shapes (Fig. 2B).

We next investigated temporal changes in irradiated MOLT-4 cells, focusing on mitochondrial membrane potential and intracellular ROS. Flow-cytometric analysis of MOLT-4 cells at 16 h after a 4 Gy irradiation identified five cell fractions (Fig. 3A): a fraction identical to unirradiated cells or viable cell fraction (R1), a low-ROS generating fraction (R2), a high-ROS generating fraction (R3), a moderate-to-high-ROS generating and low-$\Delta\psi m$ fraction (R4), and a low-ROS and low-$\Delta\psi m$ fraction (R5). Because almost all cells in the R4 and R5 fractions were stained with PI, they were considered dying or dead cells (data not shown). To elucidate the sequential process of radiation-induced cell death of MOLT-4, at 16 h after the irradiation we separated all fractions using a cell sorter and then cultured them for additional 8 h before analyzing them again by flow-cytometry. The cells that were in the R1 fraction (Fig. 3A) scattered and were found in R2, R3, R4, and R5 (Fig. 3B-R1). In a similar manner, cells in R3 remained

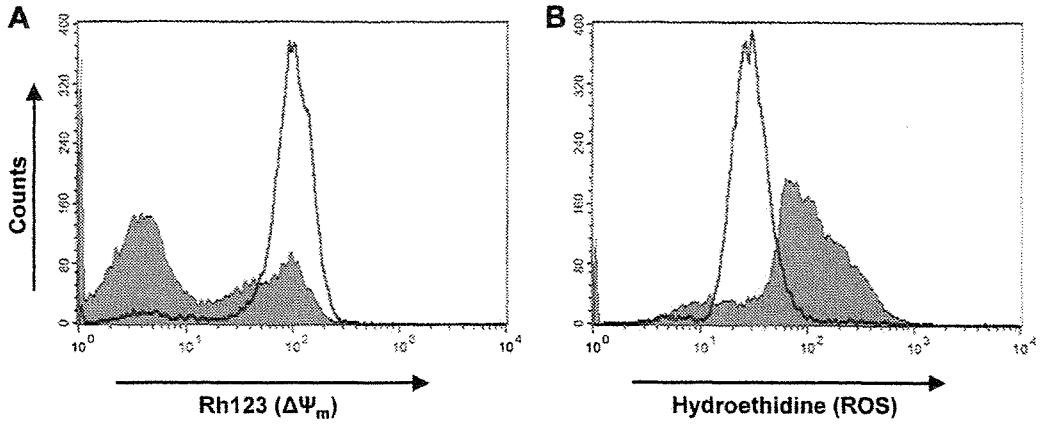

Fig. 1. Mitochondrial membrane potential and intracellular ROS in irradiated MOLT-4 cells. MOLT-4 cells were analyzed by flow-cytometry at 16 h after a 4 Gy X-ray irradiation. (A) Signal intensity of Rhodamine123 (Rh123), reflecting the membrane potential ($\Delta\psi m$), decreased in irradiated MOLT-4 cells (shaded histogram) compared with that in unirradiated cells (open histogram). (B) Hydroethidine signals represent levels of intracellular superoxide anions. The signals of irradiated cells (shaded histogram) were elevated, compared with those of unirradiated cells (open histogram).

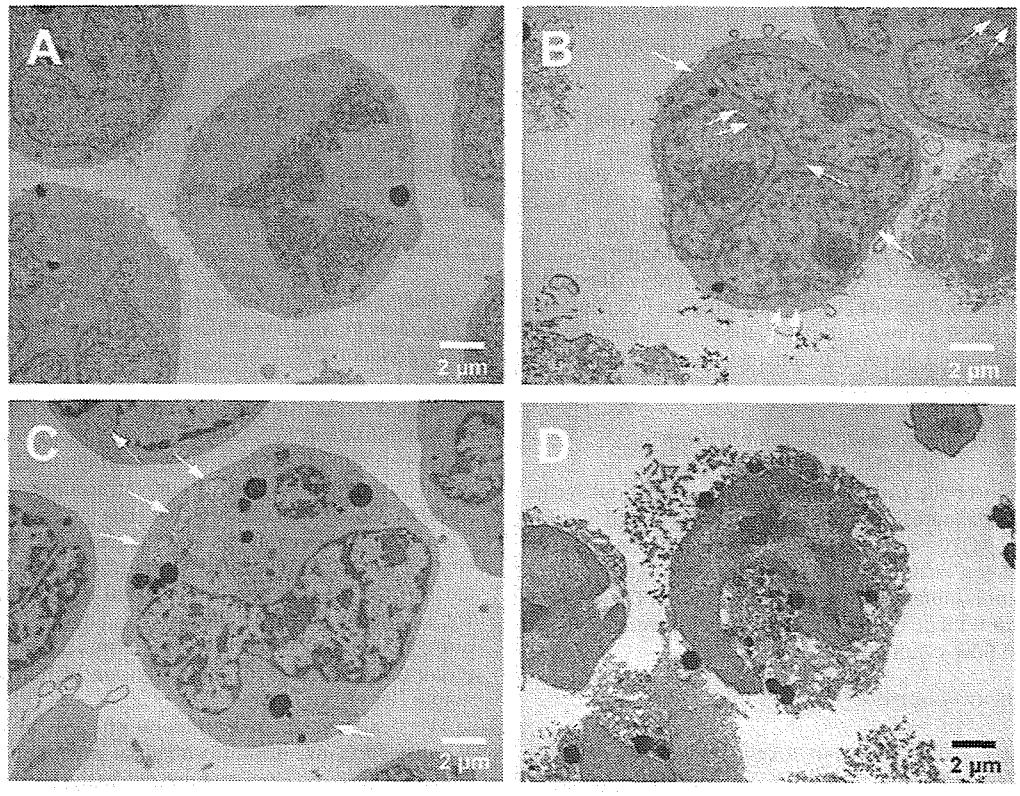

Fig. 2. Cellular morphology of irradiated MOLT-4 cells under the electron microscope. (A) Unirradiated MOLT-4 cells. (B) Irradiated MOLT-4 cells in the low-$\Delta\psi m$ R4 fraction. Normal-shaped mitochondria (indicated by white arrows) were observed at 16 h after a 4 Gy irradiation. (C and D) Irradiated MOLT-4 cells pretreated with 100 μM z-VAD-fmk in the low-ROS R2 and low-$\Delta\psi m$ R4 fractions, respectively. Swollen mitochondria (indicated by arrows) were observed at 16 h after a 4 Gy irradiation. Scale bar, 2 μm.

in R3 or moved to R4 and R5 (Fig. 3B-R3) and cells in R4 remained in R4 or moved to R5 (Fig. 3B-R4). However, cells in R2 moved only to R4 or remained in R2 (Fig. 3B-R2). It follows that most irradiated MOLT-4 cells may shift from R1 to R3, next to R4, and finally to R5; on the other hand, cells in R2 may shift to R4, and eventually R5. These observations suggest that generation of intracellular ROS is a step before a reduction of mitochondrial membrane potential in the radiation-induced apoptotic process of MOLT-4 cells.

3.2. Radiation-induced necrotic cell death of MOLT-4 without increase in intracellular ROS in the presence of a caspase inhibitor

We next investigated the involvement of caspases in X-ray-induced cell death of MOLT-4 using a broad-range caspase inhibitor, z-VAD-fmk. In the absence of z-VAD-fmk, living cell percentage of irradiated MOLT-4 cells (i.e., the cells not stained with PI) and the cell percentage of the R1 fraction were 20% and 15%, respectively, at 16 h after a 4 Gy irradiation (Fig. 4A-b, A-e, and B). In the pres-

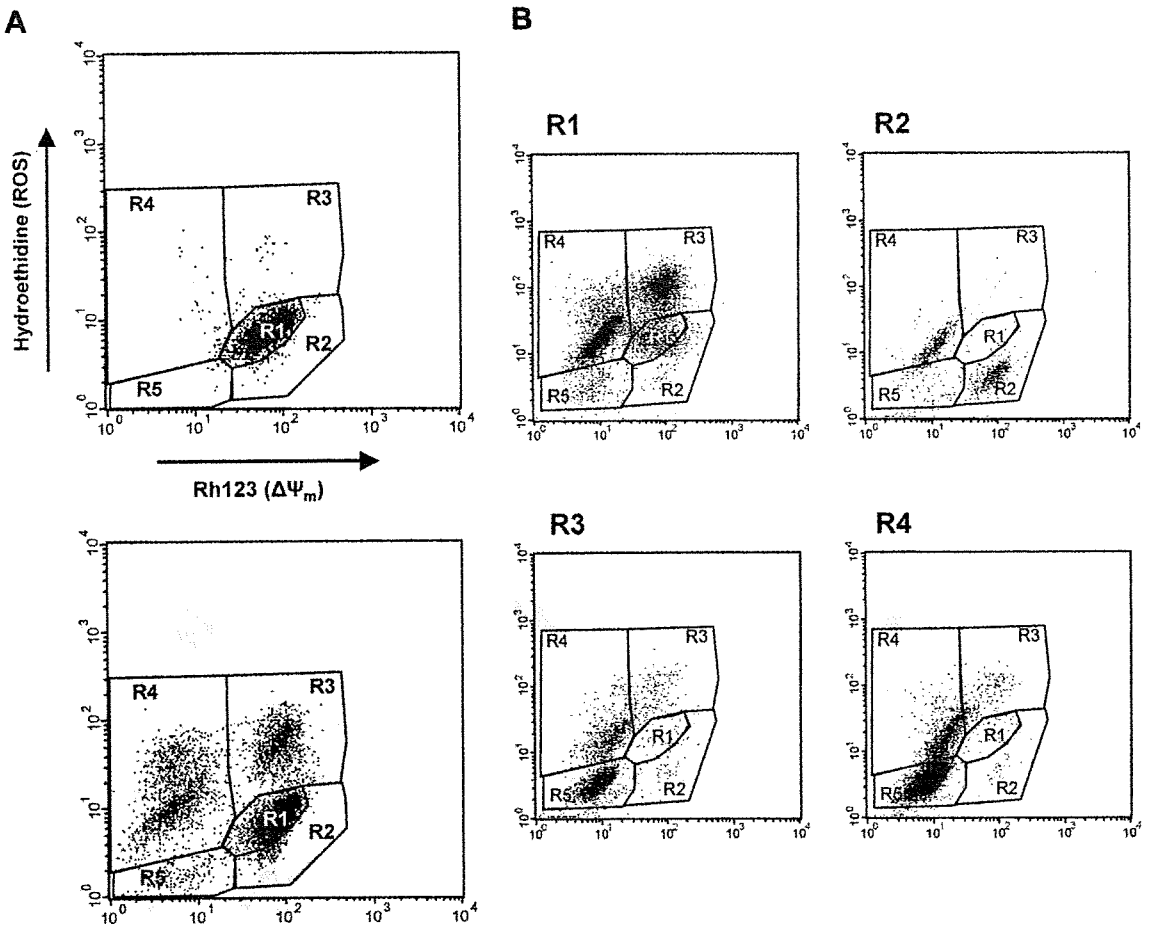

Fig. 3. Temporal changes in irradiated MOLT-4 in terms of mitochondrial membrane potential and intracellular ROS. (A) Upper and lower panels show non-irradiated control and irradiated cells, respectively. In the lower panel, five cell fractions were identified at 16 h after a 4 Gy irradiation: a viable cell fraction (R1), a low-ROS fraction (R2), a high-ROS fraction (R3), a moderate-to-high ROS and low-Δψm fraction (R4), and a low-ROS and low-Δψm fraction (R5). (B) Scattered pattern of cells in each fraction in Fig. 3A after a lapse of another 8 h. Cells in R1, R2, R3, and R4 fractions in the lower panel of Fig. 3A were isolated, cultured for another 8 h, and analyzed again by flow-cytometry.

ence of the caspase inhibitor, the percentages of living cell and the R1 fraction were 75% and 50%, respectively (Fig. 4A-c, A-f, and C). After irradiation with the z-VAD-fmk pretreatment, a number of cells were found in the R4 and R5 fractions (Fig. 4A-c), showing that cell death still occurred after caspase inhibition. Furthermore, in the case of irradiation with z-VAD-fmk, more viable cells were found in the low-ROS R2 fraction than in the high-ROS R3 fraction (Fig. 4A-c), implying that cell death occurs without excess generation of intracellular ROS. In addition, the cells in the low-ROS R2 fraction were considered to be viable, since they were not stained with PI (Fig. 4A-f).

3.3. Time-course analyses of irradiated MOLT-4 cells in the absence or presence of a caspase inhibitor

The time-course analysis clearly shows that irradiated MOLT-4 cells shifted from the R1 fraction to the partially low-ROS R2 or predominantly high-ROS R3 fraction, and eventually to the low-Δψm R4 and R5 fractions (Fig. 4B). On the other hand, cells pretreated with z-VAD-fmk traveled a different course from R1 to low-ROS R2, and eventually to low-Δψm R4 and R5, with no cells going to high-ROS R3 (Fig. 4C). In fact, when the cells in R2 were isolated and their temporal changes were analyzed by flow-cytometry, the R2 cells eventually died via R4 and R5, not R3 (data not shown).

3.4. Suppression of caspase activities by z-VAD-fmk

To confirm the suppressive effects of z-VAD-fmk in irradiated MOLT-4 cells, we next examined catalytic activity of caspases by using colorimetric substrates that mimic the cleavage sites of caspases. In the absence of z-VAD-fmk, activities of caspases—including caspase-3—were clearly enhanced by irradiation and peaked at 8 h after irradiation (Fig. 5). Up-regulation of caspase-3 expression was also confirmed by Western blotting (data not shown). In contrast, the presence of z-VAD-fmk effectively suppressed activities of all caspases examined (Fig. 5). These results were consistent with previous studies [8,20,21] which reported that caspase-3 and other caspases were activated in MOLT-4 cells following ionizing radiation. The results again demonstrated that cell death of irradiated MOLT-4 with z-VAD-fmk was independent of caspase activation.

3.5. Apoptotic and necrotic features related to cellular morphology and the cytochrome c release

We further characterized cell death in irradiated MOLT-4 with transmission electron microscopy, since its morphologic description remains the best way to discriminate apoptosis and necrosis [22]. After cells in each fraction separated with Rh123- and hydroethidine-staining were sorted, an electron microscopic review was performed. In the absence of z-VAD-fmk, mitochondria of irradi-

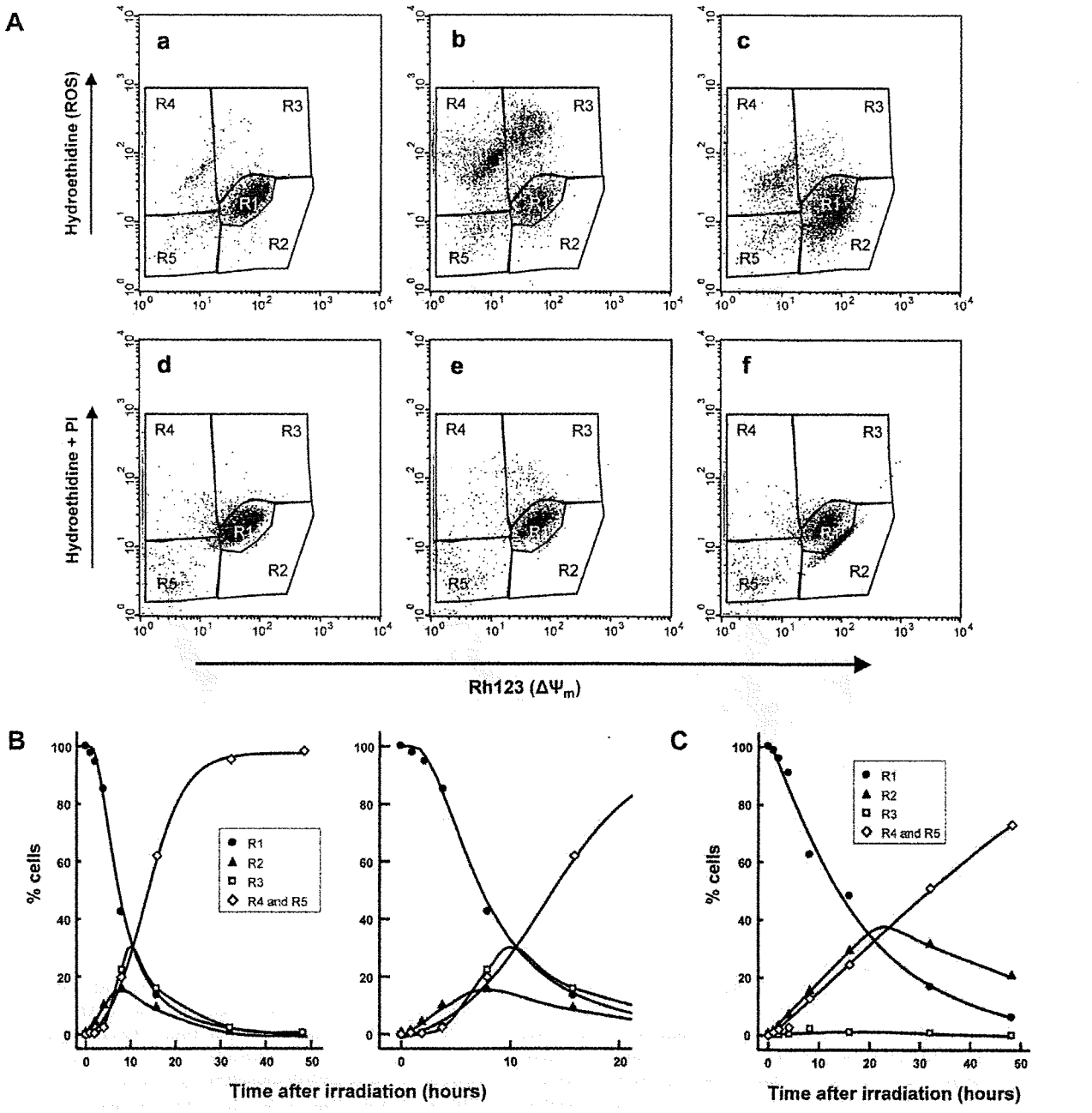

Fig. 4. Effects of caspase inhibition on radiation-induced cell death in MOLT-4. (A) Upper panels show flow-cytometric analyses with Rh123- and hydroethidine-staining on (a) unirradiated MOLT-4 cells, (b) cells at 16 h after a 4 Gy irradiation, and (c) irradiated cells pretreated with 100 μM z-VAD-fmk (note that many cells are located in the low-ROS R2 fraction). Lower panels show PI-staining in addition to Rh123- and hydroethidine-staining on (d) unirradiated cells, (e) irradiated cells, and (f) irradiated cells with z-VAD-fmk, corresponding to panels a, b, and c, respectively. In the lower panels, most PI-stained cells moved out of the displayed region due to their intense signals. (B) Time-course analyses of cells in R1 (viable cells, indicated by circle), R2 (low-ROS, triangle), R3 (high-ROS, square), and R4 and R5 (low-Δψm, rhombus) fractions after a 4 Gy irradiation. An enlarged illustration of the left panel from 0 to 20 h is shown in the right panel. (C) Time-course analyses of cells after a 4 Gy irradiation with a pretreatment with 100 μM z-VAD-fmk. Each cell fraction in Fig. 4B and C corresponds to a fraction in the upper panels of Fig. 4A.

ated MOLT-4 cells—even those in the low-Δψm R4 fraction—retained their normal shapes as already described (Fig. 2B). On the other hand, the organelles were swollen in the low-ROS R2 fraction in the presence of z-VAD-fmk (Fig. 2C). Those observations reinforced the concept that irradiated MOLT-4 cells ended in apoptosis when mediated by caspases, and necrosis proceeded under caspase inhibition. Finally, we examined cytochrome *c* release from mitochondria by flow-cytometry in order to further investigate the molecular mechanisms of radiation-induced necrosis in MOLT-4 cells. Cytochrome *c* release represents a key step in the cell death pathway, and it reportedly plays a role in radiation-induced apoptosis of MOLT-4 cells as well [23]. Cells in viable or early cell death phase, gated according to forward/side scatter properties, were analyzed with anti-cytochrome *c* antibody (clone 7H8.2C12), which binds only to mitochondrial cytochrome *c* [16]. At 16 h after a 4 Gy irradiation, the cytochrome *c* signals were significantly reduced, reflecting the release of cytochrome *c* (Fig. 6B), whereas no obvious changes in cytochrome *c* signals were detected when

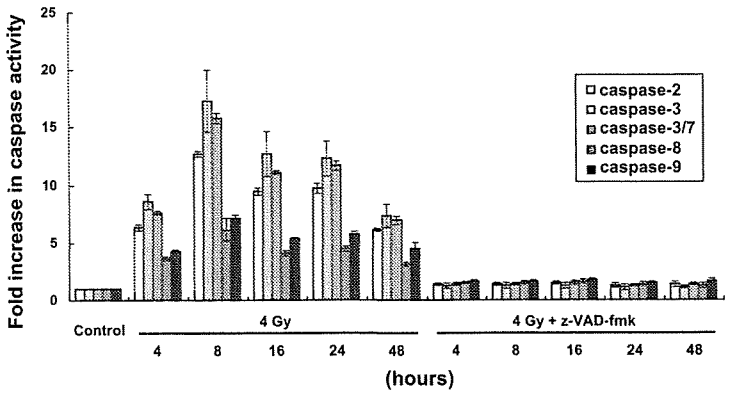

Fig. 5. Caspase activity of irradiated MOLT-4 cells in the absence or presence of a caspase inhibitor. Activities of caspases 2, 3, 3/7, 8, and 9 were examined by colorimetric assay with or without a pretreatment with 100 μM z-VAD-fmk, using fluorogenic substrates for these caspases. Fold increases in caspase activities are shown, compared with unirradiated control cells. An average of two measurements is used.

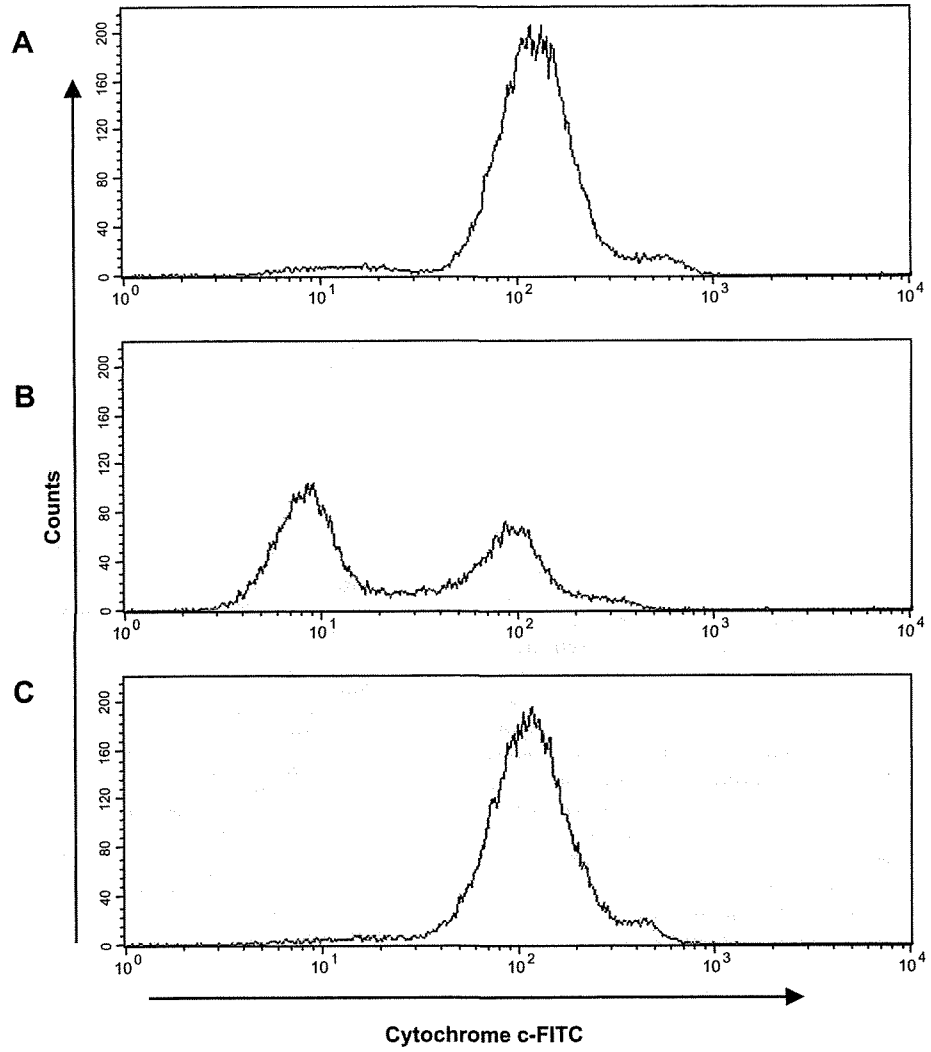

Fig. 6. Release of cytochrome *c* from mitochondria in irradiated MOLT-4 cells. Mitochondrial cytochrome *c* was detected by using anti-cytochrome *c* antibody (clone 7H8.2C12) in fixed and permeabilized MOLT-4 cells. This antibody binds only to mitochondrial cytochrome *c*, not to cytosolic one. Cells were gated according to forward/side scatter properties into viable or early phase of cell death, and then analyzed by flow-cytometry. (A) Unirradiated MOLT-4 cells. (B) MOLT-4 cells at 16 h after a 4 Gy irradiation. (C) MOLT-4 cells at 16 h after a 4 Gy irradiation in the presence of 100 μM z-VAD-fmk.

the cells were pretreated with z-VAD-fmk (Fig. 6C). These results suggest that the release of cytochrome *c* might not invariably precede necrotic cell death in irradiated MOLT-4.

4. Discussion

In the present study, apoptotic cell death was induced by a 4 Gy irradiation in MOLT-4, a thymus-derived T cell line, and the apoptosis was characterized by a decrease in mitochondrial membrane potential and an increase in intracellular ROS. On the one hand, when caspase activities were suppressed by the z-VAD-fmk pretreatment, irradiated MOLT-4 avoided apoptosis, and died exhibiting necrotic features. We demonstrated for the first time that there was no increase in intracellular ROS in the process of this necrotic cell death of MOLT-4. These results indicate that apoptosis, as the main pathway of radiation-induced cell death in MOLT-4, requires both elevation of intracellular ROS and activation of a series of caspases, while the cryptic necrosis program—independent of ROS generation and caspase activation—becomes active when the apoptosis pathway is blocked.

In agreement with our observations, this shift from apoptosis to necrosis has been reported in several cell types when the apoptosis pathways were blocked by z-VAD-fmk (U-937 cell death induced by camptothecin [24], mouse thymocyte death induced by dexamethasone and etoposide [7], and irradiated MOLT-4 cell death [8]). Enhanced expression of Bcl-2 also generated a similar shift from apoptosis to necrosis in HL-60 cells treated with oxidized low density lipoproteins [25]. In addition, interdigital cells from mice genetically lacking the caspase activator Apaf-1 underwent necrosis, not apoptosis, during embryonic development [26]. Therefore, it is plausible to imagine that cell death, including radiation-induced death, can be achieved through multiple molecular pathways—typically apoptotic or necrotic—depending on cellular physiological status and available effecter molecules.

Previous studies on radiation-induced apoptosis in MOLT-4 have suggested involvement of individual intracellular events (mediation by p53, activation of SAPK/JNK pathway, critical roles for caspase-3, modulation by Bcl-2, and occurrence of ceramide formation and PARP cleavage [8,21,23,27–29]). Even so, the sequential process of apoptosis still remains to be clarified. That is why we analyzed the temporal process of cell death in terms of mitochondrial membrane potential and intracellular ROS in this study. Our time-course analyses indicate that excess generation of ROS precedes the reduction of the membrane potential during radiation-induced apoptosis in MOLT-4 cells, whereas ROS generation is bypassed during radiation-induced necrosis. Given the potential implications of our findings, the use of antioxidants is indeed a promising strategy for prevention of radiation-induced, and ROS-dependent, cell death upon the development of radioprotective agents for cancer radiotherapy [30]. However, our findings also imply that antioxidants as radioprotective agents may be less effective for ROS-independent necrosis. Thus, development of radioprotective strategies that take into account the molecular mechanisms of ROS-independent necrosis is also warranted.

The precise mechanisms of necrosis in MOLT-4 cells remain unclear. Some previous studies have suggested the involvement of intracellular ROS generation during caspase-independent necrotic cell death, e.g., in neutrophil cells [22,31], while our and other studies have observed unaltered levels of ROS [32,33]. This discrepancy regarding ROS generation in necrotic cell death could be due to different types of cells or different experimental procedures used to induce cell death. This would imply that there are multiple pathways even in caspase-independent necrosis, both ROS-dependent and -independent. In fact, a necrotic-signaling pathway involving ROS was thought to be death receptor-mediated [22,34]. That pathway is probably distinct from the necrosis pathway of irradiated MOLT-4 found in this study, because necrosis in MOLT-4 was observed with total suppression of caspase-8, an initiation molecule for the death receptor-mediated pathway.

In addition, several non-caspase proteases, including calpain, cathepsin, and serine protease Omi/HtrA2, have been reported to be major factors in the propagation and execution phases of necrotic cell death, with or without ROS-generation [32,35–37]. Therefore, it seems certain that further studies will be needed to investigate the involvement of these non-caspase proteases in ROS-independent necrotic cell death.

Acknowledgments

The Radiation Effects Research Foundation (RERF), Hiroshima and Nagasaki, Japan is a private, non-profit foundation funded by the Japanese Ministry of Health, Labour and Welfare (MHLW) and the US Department of Energy (DOE), the latter in part through the National Academy of Sciences. This publication was supported by RERF Research Protocol 1-93 and in part by Grant-in-Aid for Scientific Research from the Ministry of Education, Culture, Sports, Science and Technology of Japan, and Grant-in-Aid for Cancer Research from the Ministry of Health, Labour and Welfare of Japan.

References

[1] S.L. Fink, B.T. Cookson, Apoptosis, pyroptosis, and necrosis: mechanistic description of dead and dying eukaryotic cells, Infect. Immun. 73 (2005) 1907–1916.
[2] G. Rainaldi, R. Romano, P. Indovina, A. Ferrante, A. Motta, P.L. Indovina, M.T. Santini, Metabolomics using 1H-NMR of apoptosis and Necrosis in HL60 leukemia cells: differences between the two types of cell death and independence from the stimulus of apoptosis used, Radiat. Res. 169 (2008) 170–180.
[3] G.M. Cohen, Caspases: the executioners of apoptosis, Biochem. J. 326 (Pt 1) (1997) 1–16.
[4] M. Enari, H. Sakahira, H. Yokoyama, K. Okawa, A. Iwamatsu, S. Nagata, A caspase-activated DNase that degrades DNA during apoptosis, and its inhibitor ICAD, Nature 391 (1998) 43–50.
[5] T. Lindsten, A.J. Ross, A. King, W.X. Zong, J.C. Rathmell, H.A. Shiels, E. Ulrich, K.G. Waymire, P. Mahar, K. Frauwirth, Y. Chen, M. Wei, V.M. Eng, D.M. Adelman, M.C. Simon, A. Ma, J.A. Golden, G. Evan, S.J. Korsmeyer, G.R. MacGregor, C.B. Thompson, The combined functions of proapoptotic Bcl-2 family members bak and bax are essential for normal development of multiple tissues, Mol. Cell 6 (2000) 1389–1399.
[6] A. Konishi, S. Shimizu, J. Hirota, T. Takao, Y. Fan, Y. Matsuoka, L. Zhang, Y. Yoneda, Y. Fujii, A.I. Skoultchi, Y. Tsujimoto, Involvement of histone H1.2 in apoptosis induced by DNA double-strand breaks, Cell 114 (2003) 673–688.
[7] T. Hirsch, P. Marchetti, S.A. Susin, B. Dallaporta, N. Zamzami, I. Marzo, M. Geuskens, G. Kroemer, The apoptosis-necrosis paradox. Apoptogenic proteases activated after mitochondrial permeability transition determine the mode of cell death, Oncogene 15 (1997) 1573–1581.
[8] D. Coelho, V. Holl, D. Weltin, T. Lacornerie, P. Magnenet, P. Dufour, P. Bischoff, Caspase-3-like activity determines the type of cell death following ionizing radiation in MOLT-4 human leukaemia cells, Br. J. Cancer 83 (2000) 642–649.
[9] P. Golstein, G. Kroemer, Cell death by necrosis: towards a molecular definition, Trends Biochem. Sci. 32 (2007) 37–43.
[10] J. Minowada, T. Onuma, G.E. Moore, Rosette-forming human lymphoid cell lines. I. Establishment and evidence for origin of thymus-derived lymphocytes, J. Natl. Cancer Inst. 49 (1972) 891–895.
[11] L.B. Chen, Mitochondrial membrane potential in living cells, Annu. Rev. Cell Biol. 4 (1988) 155–181.
[12] J.J. Ubl, J.Y. Chatton, S. Chen, J.W. Stucki, A critical evaluation of in situ measurement of mitochondrial electrical potentials in single hepatocytes, Biochim. Biophys. Acta 1276 (1996) 124–132.
[13] C. Ferlini, G. Scambia, Assay for apoptosis using the mitochondrial probes, Rhodamine123 and 10-N-nonyl acridine orange, Nat. Protoc. 2 (2007) 3111–3114.
[14] G. Rothe, G. Valet, Flow cytometric analysis of respiratory burst activity in phagocytes with hydroethidine and 2′,7′-dichlorofluorescin, J. Leukoc. Biol. 47 (1990) 440–448.
[15] S. Walrand, S. Valeix, C. Rodriguez, P. Ligot, J. Chassagne, M.P. Vasson, Flow cytometry study of polymorphonuclear neutrophil oxidative burst: a comparison of three fluorescent probes, Clin. Chim. Acta 331 (2003) 103–110.
[16] K. Stahnke, A. Mohr, J. Liu, L.H. Meyer, L. Karawajew, K.M. Debatin, Identification of deficient mitochondrial signaling in apoptosis resistant leukemia cells by flow cytometric analysis of intracellular cytochrome c, caspase-3 and apoptosis, Apoptosis 9 (2004) 457–465.

[17] X. Wang, The expanding role of mitochondria in apoptosis, Genes Dev. 15 (2001) 2922–2933.
[18] J.F. Curtin, M. Donovan, T.G. Cotter, Regulation and measurement of oxidative stress in apoptosis, J. Immunol. Methods 265 (2002) 49–72.
[19] P. Tripathi, D. Hildeman, Sensitization of T cells to apoptosis—a role for ROS?, Apoptosis 9 (2004) 515–523
[20] H. Nakano, K. Shinohara, Time sequence analysis of caspase-3-independent programmed cell death and apoptosis in X-irradiated human leukemic MOLT-4 cells, Cell Tissue Res. 310 (2002) 305–311.
[21] O. Inanami, K. Takahashi, M. Kuwabara, Attenuation of caspase-3-dependent apoptosis by Trolox post-treatment of X-irradiated MOLT-4 cells, Int. J. Radiat. Biol. 75 (1999) 155–163.
[22] W.X. Zong, C.B. Thompson, Necrotic death as a cell fate, Genes Dev. 20 (2006) 1–15.
[23] K. Takahashi, O. Inanami, M. Hayashi, M. Kuwabara, Protein synthesis-dependent apoptotic signalling pathway in X-irradiated MOLT-4 human leukaemia cell line, Int. J. Radiat. Biol. 78 (2002) 115–124.
[24] A.T. Sane, R. Bertrand, Caspase inhibition in camptothecin-treated U-937 cells is coupled with a shift from apoptosis to transient G1 arrest followed by necrotic cell death, Cancer Res. 59 (1999) 3565–3569.
[25] O. Meilhac, I. Escargueil-Blanc, J.C. Thiers, R. Salvayre, A. Negre-Salvayre, Bcl-2 alters the balance between apoptosis and necrosis, but does not prevent cell death induced by oxidized low density lipoproteins, Faseb J. 13 (1999) 485–494.
[26] M. Chautan, G. Chazal, F. Cecconi, P. Gruss, P. Golstein, Interdigital cell death can occur through a necrotic and caspase-independent pathway, Curr. Biol. 9 (1999) 967–970.
[27] H. Nakano, K. Shinohara, Correlation between unirradiated cell TP53 protein levels and radiosensitivity in MOLT-4 cells, Radiat. Res. 151 (1999) 686–693.
[28] A. Enomoto, N. Suzuki, K. Hirano, Y. Matsumoto, A. Morita, K. Sakai, H. Koyama, Involvement of SAPK/JNK pathway in X-ray-induced rapid cell death of human T-cell leukemia cell line MOLT-4, Cancer Lett. 155 (2000) 137–144.
[29] E. Takahashi, O. Inanami, T. Asanuma, M. Kuwabara, Effects of ceramide inhibition on radiation-induced apoptosis in human leukemia MOLT-4 cells, J. Radiat. Res. (Tokyo) 47 (2006) 19–25.
[30] J.F. Weiss, M.R. Landauer, Protection against ionizing radiation by antioxidant nutrients and phytochemicals, Toxicology 189 (2003) 1–20.
[31] N.A. Maianski, D. Roos, T.W. Kuijpers, Tumor necrosis factor alpha induces a caspase-independent death pathway in human neutrophils, Blood 101 (2003) 1987–1995.
[32] M. Okada, S. Adachi, T. Imai, K. Watanabe, S.Y. Toyokuni, M. Ueno, A.S. Zervos, G. Kroemer, T. Nakahata, A novel mechanism for imatinib mesylate-induced cell death of BCR-ABL-positive human leukemic cells: caspase-independent, necrosis-like programmed cell death mediated by serine protease activity, Blood 103 (2004) 2299–2307.
[33] A.S. Cowburn, J.F. White, J. Deighton, S.R. Walmsley, E.R. Chilvers, z-VAD-fmk augmentation of TNF alpha-stimulated neutrophil apoptosis is compound specific and does not involve the generation of reactive oxygen species, Blood 105 (2005) 2970–2972.
[34] A. Kawahara, Y. Ohsawa, H. Matsumura, Y. Uchiyama, S. Nagata, Caspase-independent cell killing by Fas-associated protein with death domain, J. Cell Biol. 143 (1998) 1353–1360.
[35] M. Artal-Sanz, N. Tavernarakis, Proteolytic mechanisms in necrotic cell death and neurodegeneration, FEBS Lett. 579 (2005) 3287–3296.
[36] M.J. Spencer, D.E. Croall, J.G. Tidball, Calpains are activated in necrotic fibers from mdx dystrophic mice, J. Biol. Chem. 270 (1995) 10909–10914.
[37] T. Yamashima, Ca^{2+}-dependent proteases in ischemic neuronal death: a conserved 'calpain–cathepsin cascade' from nematodes to primates, Cell Calcium 36 (2004) 285–293.

Reprint Sales Europe & ROW
Martine Cariou-Keen

Tel: +44 1865 843 845
Fax: +44 1865 843 973

m.cariou-keen@elsevier.com

Reprint Sales North America
Nicholas Pavlow

Tel: +1 212 633 3960
Fax: +1 212 462 1915

N.pavlow@elsevier.com

Neuroscience 160 (2009) 61–68

MODULATION OF CONNEXIN 43 IN ROTENONE-INDUCED MODEL OF PARKINSON'S DISEASE

A. KAWASAKI,[a,b]* T. HAYASHI,[b] K. NAKACHI,[b] J. E. TROSKO,[c] K. SUGIHARA,[a] Y. KOTAKE[a] AND S. OHTA[a]**

[a]*Graduate School of Biomedical Sciences, Hiroshima University, 1-2-3, Kasumi, Minami-ku, Hiroshima 734–8553, Japan*

[b]*Department of Radiobiology and Molecular Epidemiology, Radiation Effects Research Foundation, 5–2 Hijiyama Park, Minami Ward, Hiroshima, 732–0815, Japan*

[c]*National Food Safety Toxicology Center, Department of Pediatrics/Human Development, Michigan State University, East Lansing, MI 48824, USA*

Abstract—Gap junctional communication plays an important role in various models of brain pathology, but the changes of gap junctions in Parkinsonism are still not understood. In this study, we show that a major gap junctional protein, connexin43 (Cx43), in astrocytes is enhanced both in a rat Parkinson's disease (PD) model induced with rotenone, a widely used pesticide that inhibits mitochondrial complex I, and *in vitro* in cultured astrocytes stimulated with rotenone. Enhancement of Cx43 protein levels in rotenone-treated cultured astrocytes occurred in parallel with an increase in gap junctional intercellular communication, but was not accompanied with an increase in *Cx43* mRNA levels. Furthermore, the rotenone-induced increase of Cx43 protein levels both *in vitro* and *in vivo* was associated with increased levels of phosphorylated Cx43, which is required for gap junctional intercellular communication. In our rat PD model, phosphorylated Cx43 was selectively enhanced in the basal ganglia regions, which contain DA neurons or their terminal areas. The increase of Cx43 levels was lower in the substantia nigra pars compacta and the striatum than in the substantia nigra pars reticulata and the globus pallidus. Our findings indicate that modulation of Cx43 protein, and consequently gap junctional cellular communication, in astrocytes may play an important role in PD pathology. © 2009 IBRO. Published by Elsevier Ltd. All rights reserved.

Key words: gap junction, connexin 43, astrocyte, Parkinson's disease, dopaminergic, basal ganglia.

Parkinson's disease (PD) is an adult-onset neurodegenerative disease that is characterized by a progressive and fatal loss of dopaminergic (DA) neurons in the substantia nigra and striatum. A prototypical mitochondrial complex inhibitor, 1-methyl-4-phenyl-1,2,3,6-tetrahydropyridine, induces Parkinsonism in humans and other mammals, and systemic administration of another mitochondrial complex I inhibitor, rotenone, also causes selective death of DA neurons and Parkinsonism in rodents, accompanied by behavioral and neurochemical changes, DA degeneration, and the appearance of eosinophilic cytoplasmic inclusions (Betarbet et al., 2000). DA neurons are known to be sensitive to extracellular ions and chemical transmitters, and extracellular K^+ and glutamate were shown to play key roles in DA neuronal cell death in an animal PD model (Obata et al., 2000; Araki et al., 2001; Ransom et al., 2003). The reason why DA neurons are particularly vulnerable to complex I inhibition is not fully understood, although their vulnerability seems to be important in the development of Parkinsonism. In addition, accumulating evidence indicates an active role for nonneuronal cells, specifically astrocytes, in DA neuronal degeneration (Cardona et al., 2006; McGeer and McGeer, 2008). Astrocytes are central to maintaining the homeostatic regulation of extracellular pH, K^+, and glutamate levels (Rouach et al., 2000). However, despite the importance of astrocyte functions, the role of astrocytes in Parkinsonism remains unknown.

We have previously reported that modulation of gap junctional intercellular communication (GJIC) and connexin43 (Cx43) affect cell viability or growth, implying that GJIC may have an important role in maintaining homeostasis in various organs (Hayashi et al., 1997; Ogawa et al., 2005). It has also been reported that GJIC in astrocytes is indispensable for the homeostatic regulation of extracellular pH, K^+, and glutamate levels in the CNS (Anderson and Swanson, 2000; Ransom et al., 2003). Astrocytes are thought to be coupled by gap junctions, which consist of Cx43 (Dermietzel et al., 2000; Nagy and Rash, 2003). Alteration of Cx43 has recently been observed in ischemia, Alzheimer's disease, and Huntington's disease (Nagy et al., 1996; Vis et al., 1998; Kielian, 2008), and an increase or loss of Cx43 and GJIC in astrocytes has been observed after brain injuries and in pathogenesis associated with reactive astrocytosis (Meme et al., 2006; Haupt et al., 2007). However, whether or not altered astrocyte GJIC is involved in the development of PD remains unanswered.

Therefore, in this study we examined the changes in astrocyte GJIC and Cx43, as well as the phosphorylation status of Cx43, in a rat model of PD induced by chronic exposure to rotenone and in cultured astrocytes stimulated with rotenone. The former model has been widely used to investigate the etiology of Parkinsonism (Betarbet et al., 2000; Alam and Schmidt, 2002); the latter is useful to study

*Correspondence to: A. Kawasaki, Graduate School of Biomedical Sciences, Hiroshima University, 1-2-3, Kasumi, Minami-ku, Hiroshima 734-8553, Japan. Tel: +81-82-257-5327.
E-mail address: asamik@hiroshima-u.ac.jp (A. Kawasaki).
**Corresponding author. Tel: +81-82-257-5327.
E-mail address: sohta@hiroshima-u.ac.jp (S. Ohta).

Abbreviations: Cx43, connexin43; DA, dopaminergic; DMSO, dimethyl sulfoxide; FRAP, fluorescence recovery after photobleaching; GJIC, gap junctional intercellular communication; PBST, PBS-0.1% Triton X-100; PD, Parkinson's disease; PVDF, polyvinylidene difluoride; RR, recovery rate; SNc, substantia nigra pars compacta; SNr, substantia nigra pars reticulata; TH, tyrosine hydroxylase.

0306-4522/09 $ - see front matter
doi:10.1016/j.neuroscience.2009.01.080

the molecular mechanisms of rotenone's effects on Cx43 and GJIC.

EXPERIMENTAL PROCEDURES

Drugs and chemicals

Rotenone and dimethyl sulfoxide (DMSO) were purchased from Sigma-Aldrich (St. Louis, MO, USA). Rotenone was dissolved in DMSO (100 mM) and stored at −20 °C.

Rats

The animals were acclimated and maintained at 23 °C under a 12-h light/dark cycle (lights on 08:00–20:00 h). Rats were housed in standard laboratory cages and had free access to food and water throughout the study period. All animal experiments were carried out in accordance with the National Institutes of Health (NIH) Guide for the Care and Use of Laboratory Animals, and the protocols were approved by the Committee for Animal Research at Hiroshima University. All efforts were put in place to minimize the number of animals used and their suffering. Lewis rats (200–250 g each) were purchased from Japan SLC, Inc. (Hamamatsu, Japan). The rats were randomly divided into a rotenone group (n=6) and a control group (n=6). The rotenone group subcutaneously received rotenone (2.5 mg/kg, diluted in Panacet); the controls received vehicle (Panacet) only.

Primary astrocyte cultures

Primary astrocytes were prepared from whole brains of neonatal Wistar rats (1–2 days of age) (Hosoi et al., 2000). In brief, the brains were digested with 0.05% trypsin–EDTA (Invitrogen, Grand Island, NY, USA) at 37 °C for 10 min, and then mechanically dissociated by gentle pipetting and passed through a 70-μm-pore nylon mesh. Cells were plated onto 75 cm^2 plastic flasks and grown in DMEM (Invitrogen) supplemented with 10% v/v heat-inactivated fetal bovine serum (FBS) and 1% penicillin/streptomycin at 37 °C in a humidified 5% CO_2-containing atmosphere. The medium was changed twice a week. When cells reached confluence, at ~12 days *in vitro*, they were harvested with trypsin-EDTA (Invitrogen). Cells were then replated as a secondary culture. The purity of the primary astrocyte cultures was assessed by immunocytochemical staining, using an antibody against an astrocyte-specific marker (GFAP, dilution 1:1000; Sigma-Aldrich). At 30 days *in vitro*, 99% of the primary-cultured cells were GFAP-positive. Cultured astrocytes were treated with 0–16 nM rotenone for 48 h.

Fluorescence recovery after photobleaching (FRAP) assay for GJIC

The procedure used was a modified version of the standard method for measuring GJIC by quantitative FRAP (Wade et al., 1986; Trosko et al., 2000). Assays were performed using a Zeiss LSM 510 laser-scanning confocal microscope (Carl Zeiss International, Jena, Germany). After bleaching of randomly selected cells with a micro-laser beam, the rate of transfer of 5,6-carboxyfluorescein diacetate (Molecular Probes, Inc., Eugene, OR, USA) from adjacent labeled cells back into bleached cells was calculated. Recovery of fluorescence was examined after 0.5 min, and the recovery rate (RR) was calculated as percentage of photobleached fluorescence per min. The RR was adjusted for the loss of fluorescence measured in unbleached cells, and the results are expressed as the ratio (mean±SE) of RR to that of untreated control cells.

Extraction of Cx43 RNA

Cells were grown in 6-cm dishes and prepared as described previously (Ogawa et al., 2005). In brief, after 48 h of incubation, the cells were trypsinized and suspended in DMEM medium containing 10% FCS. Total RNA was isolated from the cells using QIAshredder and RNeasy Mini kits (Qiagen, Inc., Chatsworth, CA, USA). An initial strand of cDNA was synthesized from 500 ng of RNA extracts in a volume of 20 μl using AMV reverse transcriptase XL (TaKaRa, Otsu, Japan) priming with random 9-mers at 42 °C for 10 min. The cDNA strand was stored at −20 °C until use. Expression of *rCx43* mRNAs was evaluated by real-time RT PCR based on TaqMan methodology. In brief, PCR was performed in an ABI PRISM 7900 sequence detector (PerkinElmer/Applied Biosystems, Foster City, CA, USA) in a final volume of 20 μl. The PCR mixture contained 10 mM Tris–HCl buffer, pH 8.3 (PerkinElmer/Applied Biosystems), 50 mM KCl, 1.5 mM $MgCl_2$, 0.2 mM dNTP mixture, 0.5 U of "AmpliTaq Gold" (PerkinElmer/Applied Biosystems), 0.2 μM primers and probe. The primer and probe sequences for gene amplification were as follows: rCx43; 5-ATCAGCATCCT CTTCAAGTCTGTCT-3 (FP), 5-CAGGGA-TCTCTCTTGCA−GGTGTA-3 (RP) and 5-CC TGCTCATCCAGT-GGT-3 (probe). The "TaqMan" probe carried a 5-FAM reporter label and a 3-MGB and nonfluorescence quencher group, synthesized by Applied Biosystems. The determination of *rGAPDH* used the TaqMan rodent GAPDH control reagents (Applied Biosystems). The AmpliTaq gold enzyme was activated by heating for 10 min at 95 °C, and all genes were amplified by 50 cycles of heating for 15 s at 95 °C, followed by 1 min at 60 °C.

Quantification for *Cx43* mRNA

For the construction of standard curves of positive controls, the total RNA of primary astrocytes was reverse-transcribed into cDNA and serially diluted in water in five or six log steps to afford fourfold serial dilutions of cDNA from about 100 ng to 100 pg. These cDNA serial dilutions were prepared once for all examinations performed in this study and stored at −20 °C. The coefficient of linear regression for each standard curve was calculated, and then when the cycle threshold (CT) value of a sample was substituted in the formula for each standard curve, the relative concentration of *rCx43* or *rGAPDH* could be calculated. To normalize for differences in the amount of total RNA added to each reaction mixture, *GAPDH* was used as an endogenous RNA control. The data represent the average expression of target genes, relative to *GAPDH*, from three independent cultures.

Immunoblotting

Cells and rat brains were lysed in ice-cold lysis buffer containing 20 mM Tris-buffered saline (TBS), pH 7.5, 1% Triton X-100, 150 mM NaCl, and 1 mM each of EDTA, EGTA, β-glycerophosphate, Na_3VO_4, and phenylmethylsulfonyl fluoride, 2.5 mM sodium pyrophosphate, 1 μg/ml leupeptin. The lysates were then sonicated. The samples were diluted 1:4 in water, and their protein concentrations were determined using DC protein assay (Bio-Rad Corp., Richmond, CA, USA). Samples (10 μg) of protein were dissolved in Laemmli Sample Buffer, separated on 12.5% acrylamide gel, and transferred to polyvinylidene difluoride (PVDF) membranes (Bio-Rad). Then blots were incubated with anti-Cx43 monoclonal antibody (Chemicon International, Inc., Temecula, CA, USA) overnight at 4 °C, followed by PBS-0.1% Triton X-100 (PBST) washes three times for 15 min each. As an internal control to determine whether equal amounts of protein had been loaded on to the gel, the PVDF membranes were stripped and reprobed with anti-α-tubulin (T5168, Sigma-Aldrich). Blots were incubated with goat–antirabbit antibody–conjugated horseradish peroxidase or mouse–antimouse antibody–conjugated horseradish peroxidase. Immunoreactivity was determined by ECL detection using the ECL

plus (GE Healthcare, Piscataway, NJ, USA) according to the manufacturer's instruction.

Immunochemical staining

Antibodies against total Cx43 and phosphorylated Cx43 were used. Cells or brain sections were fixed with 4% paraformaldehyde plus 15% sucrose in PBS, pH 7.4, at room temperature for 30 min and then permeabilized with 0.1% Triton X-100 at room temperature for an additional 30 min. Nonspecific antibody binding was blocked by incubating cells with 5% bovine serum albumin (BSA) in PBS for 1 h at room temperature. Slides were incubated overnight at 4 °C with anti-Cx43 monoclonal antibody (Chemicon) at 1:500 dilution, anti-phospho-Cx43 polyclonal antibody (Cell Signaling) at 1:500 dilution, anti-GFAP antibody at 1:1000 dilution (Sigma-Aldrich), or anti-tyrosine hydroxylase (TH) polyclonal antibody (Chemicon) at 10,000 dilution. Next, the cells were washed three times with PBST and incubated with Alexa 546-conjugated goat antimouse antibody and Alexa 488-conjugated goat antirabbit antibody (Molecular Probes) at a dilution of 1:500 overnight at 4 °C, in the dark. The slides were then washed three times in PBST and once in PBS prior to being mounted in ProLong gold Antifade Reagent (Invitrogen). Finally the cells were examined using a Zeiss LSM 510 laser-scanning confocal microscope (Carl Zeiss International). Negative control, mouse or rabbit IgG was substituted for the primary antibodies.

Statistical analysis

Data were analyzed using SPSS software (version 16). The two-tailed unpaired *t*-test was used to determine the significance of mean differences between two groups.

RESULTS

Rotenone enhanced total Cx43 protein level of cultured astrocytes

Western blotting was carried out to determine whether the GJIC activity of astrocytes was related to total Cx43 protein level and/or to the extent of Cx43 phosphorylation. Three forms of Cx43 immunoreactive protein (Mr 41,000–43,000) were observed in all samples: A faster migrating band (non-phosphorylated form, P_0) and two slower migrating adjacent bands (two phosphorylated forms, P_1 and P_2; Fig. 1A). Densitometric analysis showed that rotenone induced a significant dose- and time-dependent increase of $P_0+P_1+P_2$ (total Cx43) compared with control cells (Fig. 1A, fold increase) over 6–48 h (Fig. 1A, lower panel). The effect of rotenone on *Cx43* mRNA levels was also examined, and *Cx43* mRNA levels were found not to be changed by rotenone treatment (Fig. 2).Next, we examined Cx43 localization in astrocytes, since phosphorylated Cx43, P_1 and P_2, are known to localize on the plasma membrane and gap junctions. The localization and protein levels of total Cx43 and phosphorylated Cx43 were then examined by indirect immunofluorescence cytochemistry. Fig. 1B shows immunostaining for total Cx43 (red) and phosphorylated Cx43 (green) after 48 h treatment with or without rotenone (a–d: control, a′–d′: rotenone). In control cells, total Cx43 immunoreactivity was scattered throughout the cytosol and on the plasma membrane (Fig. 1Ba), while rotenone treatment caused an increase in the distribution area and protein level of total Cx43, and the cells displayed marked linear or intermittent labeling, apparently

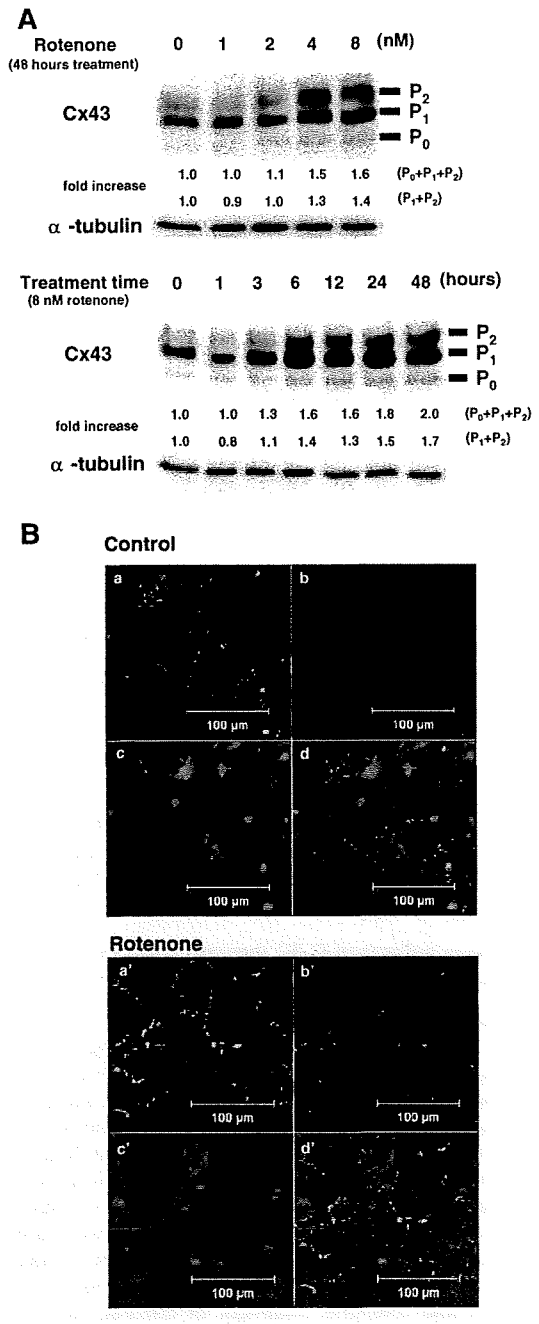

Fig. 1. Effects of rotenone on Cx43 levels. (A) Western blot analysis of Cx43 protein expression. Astrocytes were cultured with or without rotenone for 48 h at the indicated concentrations (upper panel) or with 8 nM rotenone for the indicated times (lower panel). Fold increase after culturing with rotenone is shown taking the value of untreated astrocytes as unity. (B) Intracellular localization of total Cx43 and phosphorylated Cx43 with or without 8 nM rotenone treatment for 48 h. Phosphorylated Cx43 was stained green with FITC (a, a'), and Cx43 was stained red with Cy3 (b, b'). GFAP was stained blue with Alexa 405 (c, c'). The merged image is yellow at areas of colocalization (d, d'). Images were acquired using confocal microscopy. Scale bars=100 μm.